KeA1

CHINESE ROOTS
GLOBAL IMPACT

Contents lists available at ScienceDirect

Petroleum Science





Original Paper

In-situ temperature-pressure preserved coring for onshore deep oil and gas exploration: research on the design principles and mechanical properties of the temperature-preserved core chamber



Yi-Wei Zhang ^{a, b, c}, Jia-Nan Li ^{a, c, **}, Zhi-Qiang He ^{a, c}, Ling Chen ^{a, c, d}, Cong Li ^{a, c}, Da Guo ^{a, b, c, d}, Ding-Ming Wang ^{a, b, c}, Xin Fang ^{a, b, c}, He-Ping Xie ^{a, b, c, *}

- ^a State Key Laboratory of Intelligent Construction and Healthy Operation and Maintenance of Deep Underground Engineering, College of Water Resource and Hydropower, Sichuan University, Chengdu, 610065, Sichuan, China
- ^b Guangdong Provincial Key Laboratory of Deep Earth Sciences and Geothermal Energy Exploitation and Utilization, Institute of Deep Earth Sciences and Green Energy, College of Civil and Transportation Engineering, Shenzhen University, Shenzhen, 518060, Guangdong, China
- ^c Jinping Deep Underground Frontier Science and Dark Matter Key Laboratory of Sichuan Province, Liangshan, 615000, Sichuan, China

ARTICLE INFO

Article history: Received 19 May 2024 Received in revised form 11 April 2025 Accepted 11 April 2025 Available online 11 April 2025

Edited by Jia-Jia Fei

Keywords:
In-situ coring
Temperature-pressure preserved coring
Deep oil and gas exploration
Vacuum layer
Onshore drilling

ABSTRACT

A novel temperature-preserved core chamber designed for depths exceeding 5000 m has been developed to enhance the scientific understanding of deep oil and gas reservoirs. This temperature-preserved core chamber employs an innovative vacuum layer for temperature preservation and is compatible with a temperature-pressure preserved coring system. The design principles and key parameters of the temperature-preserved core chamber were determined through static analysis. Numerical simulations assessed the mechanical properties of 70, 85, and 100 MPa core chambers under conditions of 120 –150 °C. The results demonstrate that the temperature-preserved core chambers withstand the applied stresses without plastic deformation, and the vacuum layer maintains its integrity under these conditions. A 70 MPa class core chamber prototype was manufactured, and system integration tests were performed on a self-developed in-situ coring platform. The system demonstrated stable operation at 70 MPa for 120 min, with pressure fluctuations within 5%. Additionally, the integrated system operated without interference, enabling the successful extraction of cores with a 50 mm diameter. These findings provide valuable theoretical guidance and design recommendations for advancing oil and gas in-situ temperature-pressure preserved coring technologies in high-temperature and high-pressure environments.

© 2025 The Authors. Publishing services by Elsevier B.V. on behalf of KeAi Communications Co. Ltd. This is an open access article under the CC BY-NC-ND license (http://creativecommons.org/licenses/by-nc-nd/

4.0/).

1. Introduction

Over the past century, humanity's extensive resource extraction activities have depleted shallow resources significantly, leading to a gradual shift towards deeper resource extraction (He et al., 2022). Presently, coal mining operations reach depths of up to 1500 m, geothermal mining exceeds 5000 m, metal mining ventures surpass 4350 m, and oil and gas operations penetrate depths of more than 9000 m (Xie et al., 2018). Particularly in the oil and gas

E-mail addresses: lijn2013@163.com (J.-N. Li), xiehp@szu.edu.cn (H.-P. Xie).

development sector, tapping deep-earth reservoirs has become a pivotal component of global resource strategies (Gao et al., 2022; Xie et al., 2020). In recent years, approximately 60% of the world's new oil and gas reserves have been discovered in deep formations, underscoring the vast potential of deep and ultra-deep oil and gas exploration (Guo et al., 2019; Xie et al., 2019). Notably, China has embarked on ambitious deep-earth exploration initiatives, with drilling operations for the 10,000 m deep-level wells SDTK1 and SDCK1 beginning in 2023, reflecting the country's strategic shift towards securing long-term resource reserves through deep-earth oil and gas exploration (Wang et al., 2024; Zhu et al., 2024).

The foundation of deep oil and gas development lies in accurately exploring deep resources. Coring technologies stand out as

^d School of Mechanical Engineering, Sichuan University, Chengdu, 610065, Sichuan, China

^{*} Corresponding author.

^{**} Corresponding author.

one of the most reliable and essential methods for assessing the size and characteristics of oil and gas reserves (Wang et al., 2022a). However, traditional coring technologies face significant limitations, particularly in maintaining in-situ temperature and pressure, resulting in the loss of critical data regarding subsurface formations (Xie et al., 2021). It is well established that deep oil and gas reservoirs exist under high-temperature and high-pressure conditions. which can alter the physical properties of the fluids. The changes in the in-situ environment during coring lead to distortions in key parameter such as porosity, permeability, and saturation, compromising the integrity and accuracy of the obtained cores (Hu et al., 2023; Zhang et al., 2018; Zhu et al., 2019). As a result, traditional cores fail to provide reliable compositional and stratigraphic data, undermining the precise assessment of oil and gas resources (Xie et al., 2023a). Furthermore, exploring unconventional oil and gas reservoirs often necessitates reservoir modification techniques such as fracturing and fluid replacement, which require accurate knowledge of the reservoir's physical and mechanical properties (Ma et al., 2023; Xie et al., 2023b). These highlights the pressing need to develop in-situ coring technologies to advance petroleum science (Shi et al., 2024a, 2024b).

Significant progress has been made in the development of insitu coring technologies, particularly in the field of deep-sea gas hydrate exploration. The initial breakthrough came with in-situ pressure-preserved coring (IPP-Coring) technologies, such as the Pressure Core Tube (PCB) used in the Deep Sea Drilling Program (DSDP), which could maintain pressures of up to 35 MPa (Kvenvolden et al., 1983). Later, the Pressure Core Sampler (PCS) developed for the Ocean Drilling Program (ODP) increased pressure preservation capabilities to 70 MPa (Dickens et al., 1997; Milkov et al., 2004). The European Union also developed the HYACE system, including the Fugro Pressure Corer (FPC) and the HYACE rotary corer (HRC), which could preserve pressures up to 25 MPa (Schultheiss et al., 2009). However, these technologies could not preserve the in-situ temperature of the core, which would often revert to ambient conditions, leading to a loss of in-situ pressure as well. To address this, in-situ temperature-preserved coring (ITP-Coring) technologies were developed. Notable examples include the Pressure Tight Piston Corer (PTPC) from Zhejiang University, which employs electroplated insulation to preserve temperatures and maintain pressure up to 30 MPa (Qin et al., 2005). The thermoelectric cooling system used by Japan Oil, Gas, and Metals Corporation (JOGMEC) suppresses temperature fluctuations and can preserve pressures up to 24.1 MPa (Kawasaki et al., 2006). Additionally, the Chinese Academy of Geological Sciences developed the in-situ sampler for gas hydrate filled with thermal insulation material in a vacuum core tube and cooled by a semiconductor chiller, capable of maintaining pressures up to 30 MPa (Zhang et al., 2007b). Further advancements in temperature-preserved systems have included the Dynamic Autoclave Piston Cover (DAPC) and the Multiple Autoclave Cover (MAC) developed in Germany, both of which utilize cold sources to maintain temperature, with pressure preservation capacities of 20 and 14 MPa, respectively (Abegg et al., 2008). The pressure and temperature-preserved system (PTPS) invented by China University of Petroleum (Beijing) employs thermal insulation coats, insulation materials, and vacuum layers to control temperature, allowing for pressure preservation of up to 30 MPa (Zhu et al., 2011).

China's exploration of onshore deep oil and gas extraction utilizing in-situ coring technology has progressed significantly in recent years. Daqing Oilfield spearheaded the development of the BYM series of pressure-preserved coring tools, with the flagship being the BYM-III coring tool, capable of withstanding pressures of

up to 40 MPa (Zhang et al., 2007a). The China National Petroleum Corporation Great Wall Drilling Co. Ltd. further advanced these technologies with the GW-CP194-80 A, which can handle pressures up to 60 MPa for conventional and unconventional reservoirs (Yang et al., 2020). The Beijing Institute of Prospecting Engineering also developed the TKP194-80 pressure-preserved coring tool for coalbed methane exploration, with a pressure tolerance of 50 MPa (Zhao et al., 2023). Additionally, notable progress has been made in ITP-Coring technologies. The GW-CP194-70 BB developed by the Great Wall Drilling employs vacuum-insulated cylinders to preserve both temperature and pressure, with a maximum pressure preservation capacity of 20 MPa (Yang et al., 2014). Also noteworthy are the heat-pressure-shape-preserved coring tools for coalbed methane and dense sandstone using thermal insulation materials and vacuum layers (Wang et al., 2022b, 2021). They demonstrate remarkable pressure resilience, with a maximum tolerance of up to 60 MPa.

A brief comparison of typical existing in-situ coring techniques is presented in Table 1. Despite these advancements, existing in-situ coring technologies face challenges when applied to deeper formations. For instance, while deep-sea gas hydrate in-situ pressurepreserved coring technologies can achieve a pressure preservation capacity of up to 70 MPa, the combined pressure-temperature preservation capacity is limited to 30 MPa. This suggests that integrating temperature-preserved coring technology may compromise the pressure resistance of current systems. Furthermore, existing onshore oil and gas in-situ temperature-pressure preserved coring technologies have a maximum pressurepreserved capacity of 60 MPa. When it comes to temperaturepreserved techniques, two main strategies are commonly employed: passive techniques and active techniques. Passive techniques rely on vacuum layers, thermal insulation coatings, and materials designed for thermal insulation. On the other hand, active techniques involve mechanisms like thermoelectric and cold source refrigeration to regulate and maintain desired temperatures actively.

However, the current research is aimed at deep ocean or onshore deep wells less than 5000 m deep. Challenges arise as onshore deep oil and gas coring enters deeper formations, including:

- (1) **High temperature-pressure coupling environments:** At depths beyond 5000 m, pressures exceeding 70 MPa are inevitable, exceeding the capabilities of current in-situ temperature-pressure preserved technologies. Besides, the high-temperature environment of the deep well, which is different from the low-temperature environment of the deep ocean, limits the active temperature-preserved techniques. For example, it is difficult to set up cables for electric heating at the shaft bottom, and chips may fail to function properly at the well temperature.
- (2) Narrow borehole dimensions: As coring depths increase, borehole diameter decrease, with the diameter at 5000 m as small as 215.9 mm, thus limiting the thickness of coring tools.
- (3) High coring efficiency: Because of the strict well control requirements in onshore deep oil and gas coring, lifting drill coring technology is used instead of wireline coring technology (Guo et al., 2023a). However, to ensure high coring efficiency, the single-time coring length in lifting drill coring technology is typically twice or three times longer than in wireline coring technology. Therefore, the coring tools exhibit long and narrow geometric characteristics, and

 Table 1

 Comparison of different typical existing in-situ coring techniques.

Coring technology	Pressure	Temperature	Coring type
FPC	≤25 MPa		Deep sea gas hydrates
HRC	≤25 MPa	_	
PCB	≤35 MPa	_	
PCS	≤70 MPa	_	
MAC	≤14 MPa	Cold source	
DAPC	≤20 MPa	Cold source	
PTCS	≤24.1 MPa	Thermoelectric cooling technology	
PTPC	≤30 MPa	Electroplated insulation material	
PTPS	≤30 MPa	Vacuum	
		Thermal insulation coats	
		Insulation materials	
In-situ sampler for gas hydrate	≤30 MPa	Thermal insulation material	
. ,		Semiconductor chillers	
BYM-III	≤40 MPa		Onshore oil and gas
TKP194-80	≤50 MPa	_	_
GW-CP194-80 A	≤60 MPa	_	
GW-CP194-70BB	<20 MPa	Vacuum	
Heat-pressure-shape-preserved coring tool for coalbed methane	≤60 MPa	Thermal insulation material	
Heat-pressure-shape-preserved coring tool for dense sandstone	_ ≤60 MPa	Vacuum	
	_	Thermal insulation material	

unreasonable design would result in unacceptable stress and deformation.

This paper presented a newly developed temperature-preserved core chamber suitable for the in-situ temperature-pressure preserved coring system to tackle the abovementioned challenges and fulfill the demands of onshore deep-well oil and gas coring. The structure design principles under different temperature-pressure couplings were obtained through theoretical calculations. Furthermore, the mechanical properties of the temperature-preserved core chamber were assessed via numerical simulations. Based on the above results, a 70 MPa class prototype was produced and integrated into the in-situ temperature-pressure preserved coring system, undergoing rigorous pressure resistance and coring function tests. Theoretical guidance and design principles for in-situ temperature-pressure preserved coring systems aimed at deep oil and gas exploration beyond 5000 m are provided by this study.

2. Composition and working principle of in-situ temperature-pressure preserved coring system

To address the increasing demands for deep oil and gas exploration and development, we have advanced the in-situ temperature-pressure preserved coring system by integrating a temperature-preserved core chamber with the previously designed IPP-coring tool, as described in the literature (Guo et al., 2023b). The composition of the coring system is illustrated in Fig. 1. At the top of the system, as shown in Fig. 1(a), is a hydrodynamic-driven differential motion assembly acting as a power lifting device. The lower end of this assembly is connected to the core tube, which passes through the interior of the temperature-preserved core chamber. A pressure controller is positioned at the lower end of the core tube. These components are encased within the outer pipe, with the coring bit attached to the bottom of the system and connected to the outer pipe.

The structure and working principle of the temperature-preserved core chamber are shown in Fig. 1(b). This chamber employs a double-cylinder fit design, which utilizes the vacuum's low static air thermal conductivity (0.023 W/(m·K)). Compared to other insulation materials, vacuum insulation demonstrates superior thermal resistance, as detailed in Table 2 (He et al., 2024; Şeker et al., 2022; Yang et al., 2022). Besides, the vacuum insulation

method does not require a power supply like the active temperature-preserved techniques (Xue et al., 2023). The vacuum layer, formed between the two cylinders, is the primary barrier to heat transfer. Sealing rings are placed within grooves at both ends of the inner cylinder to prevent vacuum leakage. Moreover, antiradiation material is coated on the inner surface of the vacuum layer to insulate heat radiation.

The working principle of the in-situ temperature-pressure preserved coring system is illustrated in Fig. 2. As shown in Fig. 2(a), the coring system first descends to the target formation, where coring operations begin. During the downhole procedure, density mud is pumped into the annular space between the temperaturepreserved core chamber and the outer pipe. As shown in Fig. 2(b), once the prescribed coring depth is reached, the differential motion assembly is triggered to lift the core tube containing the in-situ core, moving it into the temperature-preserved core chamber. The pressure controller is activated to seal the system once the core tube is fully raised. Temperature and pressure preservation are then independently managed by the temperaturepreserved core chamber and the pressure controller. The in-situ core is thus protected within the temperature-preserved core chamber, maintaining its original temperature and pressure conditions. Upon completion of the coring operation, the entire system is hoisted back to the surface, bringing the coring process to a close.

This design ensures that the in-situ core is preserved under the target formation's specific temperature and pressure conditions, facilitating more accurate analysis and assessment of deep oil and gas resources.

3. Design principles of the temperature-preserved core chamber

The reliability and functionality of the temperature-preserved core chamber must be assured under extreme in-situ conditions during the coring process. This section outlines the design principles for the temperature-preserved core chamber, including the derivation of yield equations from the Lamé equation and distortion energy theory. These principles guide the design methodology and parameter calculations for the temperature-preserved core chamber under varying in-situ environmental conditions.

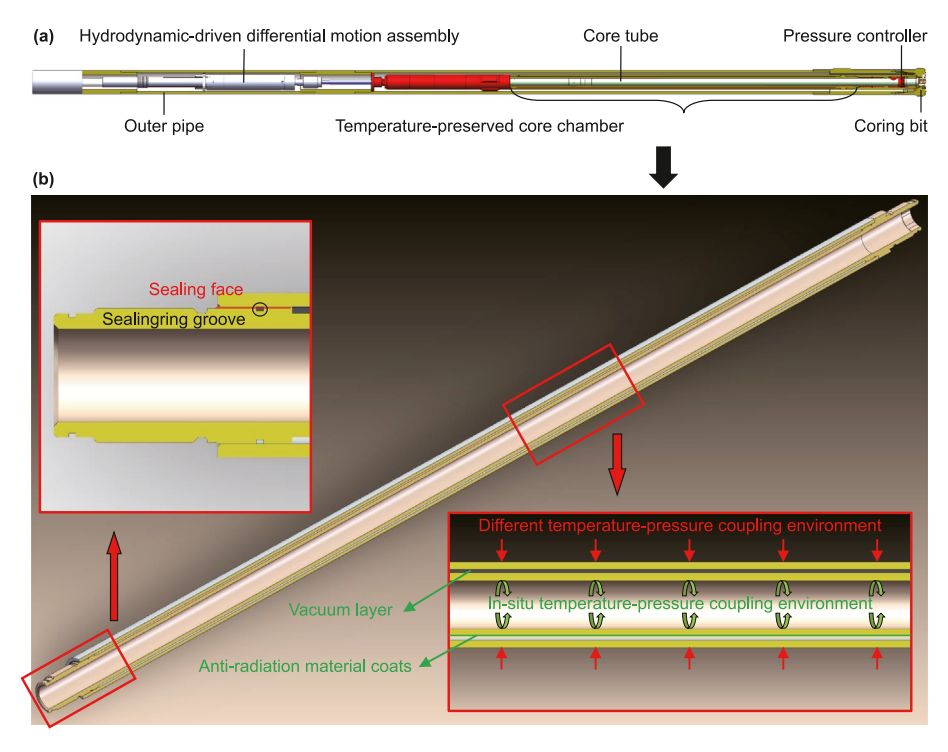


Fig. 1. (a) Composition of the in-situ temperature-pressure preserved coring system; (b) structure and working principle of the temperature-preserved core chamber.

Table 2Comparison of thermal conductivity of different thermal insulation materials.

Thermal insulation material	Thermal conductivity, $W/(m \cdot K)$
Vacuum	<0.023
Glass wool	0.032-0.049
Foam glass	0.056-0.064
Foam concrete	0.060-0.069
Rock wool	<0.076

3.1. Mathematical modeling assumptions

In engineering applications, the temperature-pressure preserved coring system for deep oil and gas exploration is subjected to

combined influences of formation temperature and pressure. Given the relatively small size of the temperature-preserved core chamber compared to the surrounding formation, temperature and pressure gradients along its axial direction are minimal. As the system is lowered from the wellhead to the target formation, the temperature and pressure within the temperature-preserved core chamber vary with depth. However, during coring operations at the bottom of the well, the temperature-preserved core chamber can be assumed to encounter uniform temperature and pressure conditions due to minimal depth changes.

Thus, based on these engineering considerations, the temperature-preserved core chamber can be mathematically modelled with the following assumptions:

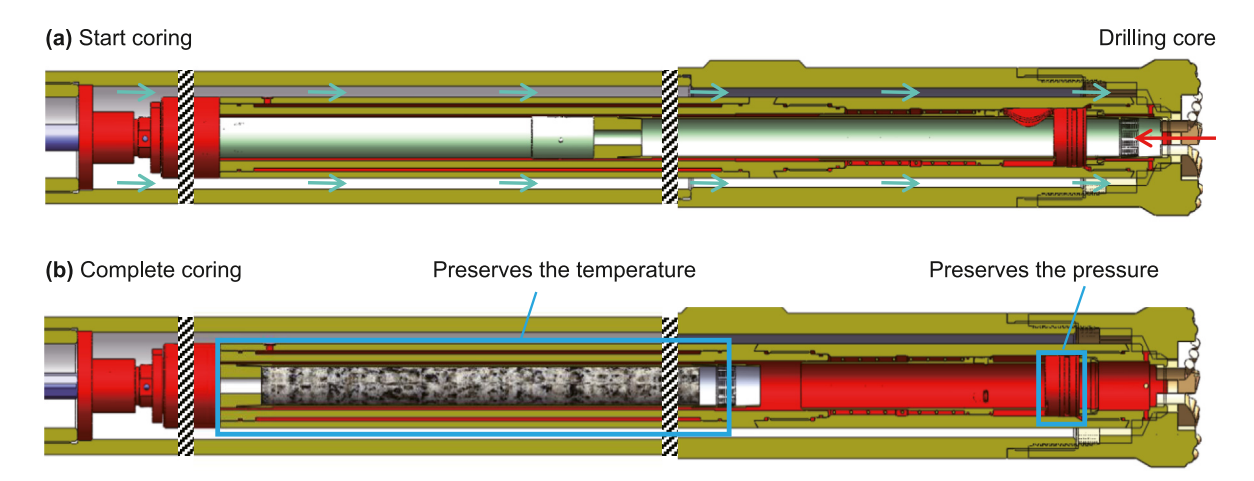


Fig. 2. Working principle of the in-situ temperature-pressure preserved coring system: (a) system lowered to the target formation for coring; (b) in-situ core lifted to the temperature-preserved core chamber, pressure controller closes.

- (1) **Material behaviour:** The material is assumed to exhibit elastic-plastic behaviour, with elastic deformation conforming to Hooke's law and the small deformation hypothesis.
- (2) Material properties: The elastic modulus, Poisson's ratio, thermal conductivity, and coefficient of thermal expansion are assumed to remain constant within the specified temperature range.
- (3) Coupling calculation method: Temperature-displacement coupling is assumed to be direct, and the thermoelastic problem is considered to exhibit steady-state heat conduction.
- (4) **Pressure and temperature fields:** Pressure and temperature fields are assumed to be uniform along the chamber's axial direction, with axisymmetric distributions of these parameters.

3.2. Theoretical analysis of core chamber bearing characteristics

A simplified mathematical model of the temperature-preserved core chamber is developed based on the aforementioned assumptions. Under assumptions (1), (2), and (4), the chamber is conceptualized as a system of two concentric cylinders. The outer and inner radius are denoted as R_0 and R_i , respectively, and the ratio K of these radius is defined as:

$$K = \frac{R_0}{R_i} \tag{1}$$

If K<1.1, the cylinder is classified as thin-walled; otherwise, it is treated as thick-walled (Júnior et al., 2023). Thick-walled cylinders, subjected to uniform internal and external pressures, require a three-dimensional stress analysis, governed by the Lamé equations:

$$\sigma_{\theta} = \frac{p_{i}R_{i}^{2} - p_{o}R_{o}^{2}}{R_{o}^{2} - R_{i}^{2}} + \frac{(p_{i} - p_{o})R_{i}^{2}R_{o}^{2}}{R_{o}^{2} - R_{i}^{2}} \frac{1}{r^{2}}$$
(2)

$$\sigma_r = \frac{p_i R_i^2 - p_o R_o^2}{R_o^2 - R_i^2} - \frac{(p_i - p_o) R_i^2 R_o^2}{R_o^2 - R_i^2} \frac{1}{r^2}$$
(3)

$$\sigma_{z} = \frac{p_{i}R_{i}^{2} - p_{o}R_{o}^{2}}{R_{o}^{2} - R_{i}^{2}} \tag{4}$$

where σ_{θ} , σ_r , and σ_z represent the circumferential, radial, and axial stresses, respectively; p_i and p_o are the internal and external pressures; r is the radius of any point on the cylinder.

When the inner cylinder of the temperature-preserved core chamber is threaded at both ends, it is assumed to be constrained by the closure and axial rigidity at both ends, such that axial strain ε_Z is zero, and axial stress σ_Z satisfies the following equation:

$$\sigma_z = 2\mu \frac{p_i R_i^2 - p_0 R_0^2}{R_0^2 - R_i^2} \tag{5}$$

where μ is Poisson's ratio.

The radial stress is much smaller than the axial and circumferential stresses for thin-walled cylinders under uniform internal or external pressure. Therefore, it is reasonable to assume that each point in the cylinder experiences a two-way stress state,

represented by:

$$\sigma_{\theta} = \frac{pD}{2\delta} \tag{6}$$

$$\sigma_z = \frac{pD}{4\delta} \tag{7}$$

where D is the midplane diameter of the wall and δ is the thickness of the wall, which satisfy the following geometric relationship:

$$D = R_0 + R_i \tag{8}$$

$$\delta = R_0 - R_i \tag{9}$$

Given assumptions (3) and (4), thermal stresses within the temperature-preserved core chamber are modelled by:

$$\sigma_{z}^{T} = -\alpha E \Delta T \tag{10}$$

where α is the coefficient of linear thermal expansion; E is the modulus of elasticity; ΔT is the temperature change.

The equations above elucidate the stresses induced within the temperature-preserved core chamber. Given the simultaneous application of temperature and pressure loads, it is imperative to employ strength theory to ascertain the yielding of the chamber. The distortion energy theory posits that the deformation-induced specific energy $u_{\rm d}$ primarily contributes to material yield damage. Consequently, yielding transpires when $u_{\rm d}$ attains a threshold where material yield occurs under uniaxial tensile stress. Within temperature-preserved core chambers, yielding arises when the resultant equivalent force $\sigma_{\rm eq}$ surpasses the yield strength of the material. The following equation governs the resultant equivalent force:

$$\sigma_{eq} = \sqrt{\frac{\left(\sum \sigma_r - \sum \sigma_\theta\right)^2 + \left(\sum \sigma_r - \sum \sigma_z\right)^2 + \left(\sum \sigma_\theta - \sum \sigma_z\right)^2}{2}} \tag{11}$$

When the maximum stress point of the temperature-preserved core chamber enters the plasticity, the corresponding load is called the initial yield load p_s . When the temperature-preserved core chamber is subjected to loads exceeding the initial yield load, local plastic deformation occurs within the chamber body, and a residual stress field is established once the load is removed. Upon the temperature-preserved core chamber re-entry into the well, if the combined stress from the temperature-pressure load and the residual stress exceeds the yield load, the accumulation of plastic deformation could lead to a loss of stability in the temperature-preserved core chamber. The design should avoid plastic deformation since the temperature-preserved core chamber is subject to cyclic loading over extended periods. Therefore, the elastic-plastic failure design criterion was adopted, and it is considered that the temperature-preserved core chamber fails when the load reaches the initial yield load.

When analyzing thick-walled cylinders, the inner wall surfaces yield first under internal pressure alone. The internal pressure p_i and the inner wall surface radius r can be expressed as p_s and R_i respectively. Referring to Eqs. (2), (3), (5) and (11), the yield function for the thick-walled inner cylinder is as follows:

$$f_{i}(p_{s}, \Delta T, K) = \sigma_{Re} - \sqrt{\frac{\left(-p_{s}\frac{2K^{2}}{K^{2}-1}\right)^{2} + \left(-p_{s}\frac{K^{2}-1+2\mu}{K^{2}-1} + \alpha E \Delta T\right)^{2} + \left(p_{s}\frac{K^{2}+1-2\mu}{K^{2}-1} + \alpha E \Delta T\right)^{2}}{2}}$$
(12)

where σ_{Re} is the yield strength of the material.

Similarly, the inner wall is the first to yield if the external pressure acts alone. The inner wall surface's external pressure and radius can be represented as p_s and R_i , respectively. The yield function for the thick-walled outer cylinder is expressed using Eqs. (2)–(4) and (11) as follows:

$$f_{\rm o}(p_{\rm s}, \Delta T, K) = \sigma_{\rm Re}$$

$$-\sqrt{\frac{\left(p_{s}\frac{2K^{2}}{K^{2}-1}\right)^{2}+\left(p_{s}\frac{K^{2}}{K^{2}-1}+\alpha E\Delta T\right)^{2}+\left(-p_{s}\frac{K^{2}}{K^{2}-1}+\alpha E\Delta T\right)^{2}}{2}}$$
(13)

when considering thin-walled cylinders, the yield function can be obtained using Eqs. (6), (7) and (11):

$$f(p_s, \Delta T, K) = \sigma_{Re} - \sqrt{\frac{3p_s^2}{16} \left(\frac{K+1}{K-1}\right)^2 + (\alpha E \Delta T)^2}$$
 (14)

when the yield function value equals zero, the corresponding diameter ratio K is considered the design diameter ratio of the temperature-preserved core chamber.

Furthermore, it is essential to consider the stability of the pressure cylinder. For thin-walled cylinders, axial bifurcation buckling occurs when the axial uniform compression load becomes excessive. Therefore, the axial load of the thin-walled cylinder should not exceed the critical stress, as given by:

$$\sigma_{\rm cr} = \frac{1}{\sqrt{3(1-\mu^2)}} \frac{2E\delta}{D} \tag{15}$$

where σ_{cr} is the critical stress.

In this study, the axial stress in the thin-walled cylinder includes both thermal stress and axial tension induced by uniform external pressure. Referring to Eqs. (7), (10) and (15), the axial stability conditions of thin-walled cylinders can be derived as:

$$p_{\rm s} \left(\frac{K+1}{K-1}\right)^2 - 4\alpha E \Delta T \frac{K+1}{K-1} \le \frac{8E}{\sqrt{3\left(1-\mu^2\right)}} \tag{16}$$

When cylinders are subjected to uniform external pressure, circumferential stability must also be considered. Based on the critical length formula (Eq. (17)), it is evident that the cylinders studied in this research are long cylinders. Excessive external pressure can lead to pressure instability in the middle of the cylinder. Consequently, the uniform external pressure should satisfy the following conditions:

$$L_{\rm cr} = 1.17D\sqrt{\frac{\overline{D}}{\delta}} \tag{17}$$

$$p_{\rm s} \le \frac{2E}{1 - \mu^2} \left(\frac{\delta}{D}\right)^3 \tag{18}$$

Table 3 Theoretical equations for the bearing characteristics of the temperature-preserved core chamber.

a) Thin-walled cylinders

a-1) Subjected to uniform external pressure and thermal load

The yield function: $f(p_s, \Delta T, K) = \sigma_{\text{Re}} - \sqrt{\frac{3p_s^2}{16} \left(\frac{K+1}{K-1}\right)^2 + (\alpha E \Delta T)^2}$

Axial stability criterion: $p_s \left(\frac{K+1}{K-1}\right)^2 - 4\alpha E\Delta T \frac{K+1}{K-1} \le \frac{8E}{\sqrt{3(1-\mu^2)}}$

Circumferential stability criterion: $p_s \le \frac{2E}{1-\mu^2} \left(\frac{K-1}{K+1}\right)$

a-2) Subjected to uniform internal pressure and thermal load

The yield function: $f(p_s, \Delta T, K) = \sigma_{\rm Re} - \sqrt{\frac{3p_s^2}{16} \left(\frac{K+1}{K-1}\right)^2 + (\alpha E \Delta T)^2}$

Axial stability criterion: $p_s\left(\frac{K+1}{K-1}\right)^2 - 4\alpha E\Delta T \frac{K+1}{K-1} \le \frac{8E}{\sqrt{3(1-\mu^2)}}$

b) Thick-walled cylinders

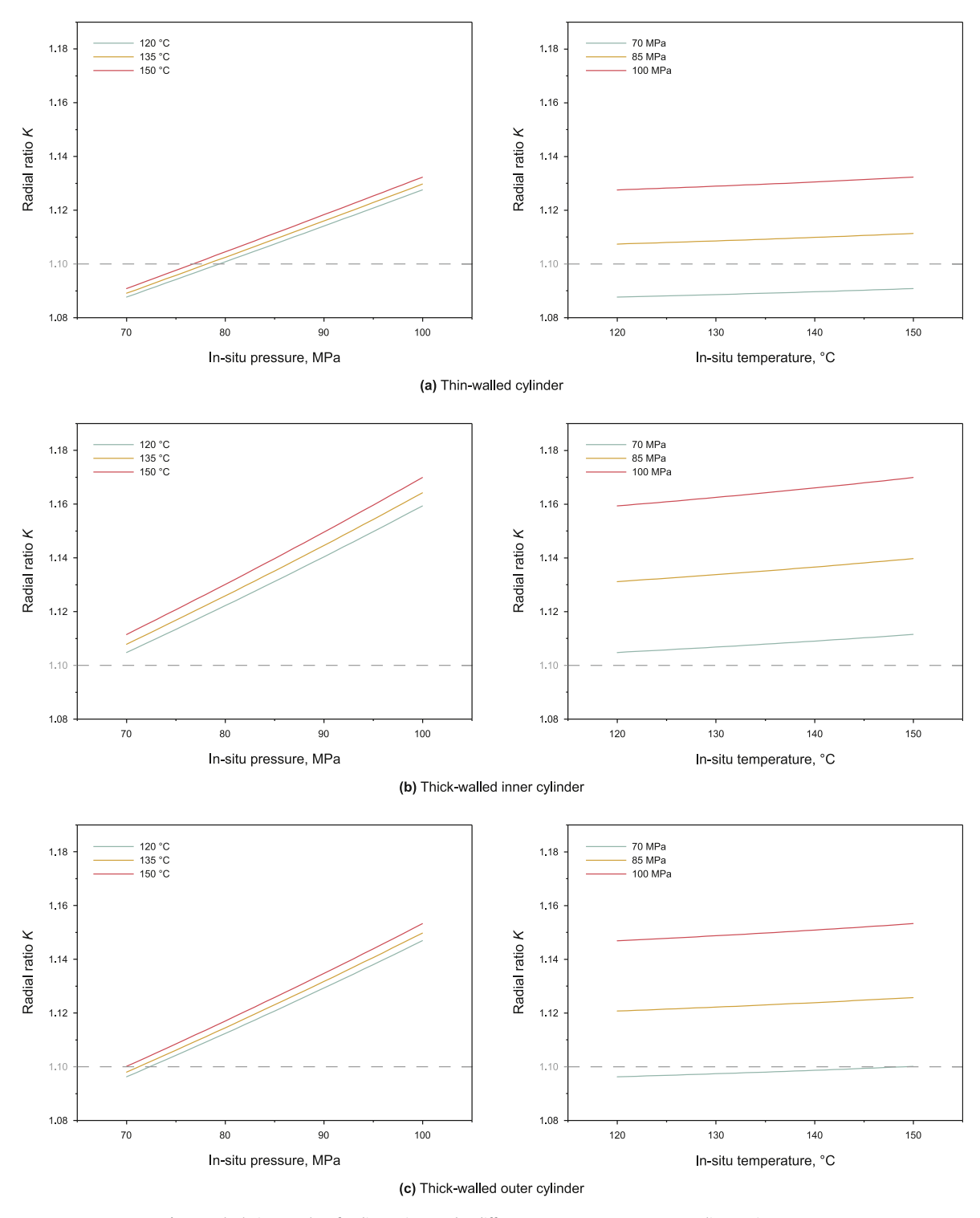
b-1) Subjected to uniform external pressure and thermal load

The yield function: $f_0(p_s, \Delta T, K) = \sigma_{\text{Re}} - \sqrt{\frac{\left(p_s \frac{2K^2}{K^2 - 1}\right)^2 + \left(p_s \frac{K^2}{K^2 - 1} + \alpha E \Delta T\right)^2 + \left(-p_s \frac{K^2}{K^2 - 1} + \alpha E \Delta T\right)^2}$

Circumferential stability criterion: $p_s \le \frac{2E}{1-\mu^2} \left(\frac{K-1}{2K}\right)$

b-2) Subjected to uniform internal pressure and thermal load

$$\text{The yield function: } f_i(p_s, \Delta T, K) \ = \ \sigma_{\text{Re}} - \sqrt{\frac{\left(-p_s \frac{2K^2}{K^2-1}\right)^2 + \left(-p_s \frac{K^2-1+2\mu}{K^2-1} + \alpha E \Delta T\right)^2 + \left(p_s \frac{K^2+1-2\mu}{K^2-1} + \alpha E \Delta T\right)^2}{2}}$$



 $\textbf{Fig. 3.} \ \ \textbf{Calculation results of radius ratio} \ \textit{K} \ \textbf{under different temperature-pressure coupling environments}.$

where L_{cr} is the critical length.

Finally, considering the effects of uniform pressure and temperature variations on the strength and stiffness of the temperature-preserved core chamber, the theoretical analysis equations of the temperature-preserved core chamber bearing characteristics are summarized in Table 3.

3.3. Design schemes and parameter calculations

Both domestic and foreign research on coring tools for onshore deep oil and gas reservoirs has reached a mature stage within the pressure range of 60 MPa. In this paper, the design of the temperature-preserved core chamber is based on the temperature-pressure coupling conditions at depths exceeding 5000 m. The pressure amplitude ranges from 70 to 100 MPa, and the

temperature fluctuates between 120 and 150 °C. For boreholes deeper than 5000 m, with a diameter less than 215.9 mm, the temperature-preserved core chamber's outer annulus must meet the requirements for mud passage, as illustrated in Fig. 2. Hence, the maximum outer diameter of the outer cylinder is constrained to 110 mm. Additionally, the interior of the chamber must facilitate smooth initiation and completion of coring actions, such as the operation of the pressure controller flip. Consequently, the minimum inner diameter of the inner cylinder is set at 62.5 mm. Nine critical temperature-pressure coupling conditions were investigated, with in-situ temperatures set at 120, 135, and 150 °C and insitu pressures at 70, 85, and 100 MPa. The pressure safety factor is set at 1.1. The diameter ratio *K*, under those different temperature-pressure coupling conditions, was computed using yield functions (12), (13), and (14), and the results are depicted in Fig. 3.

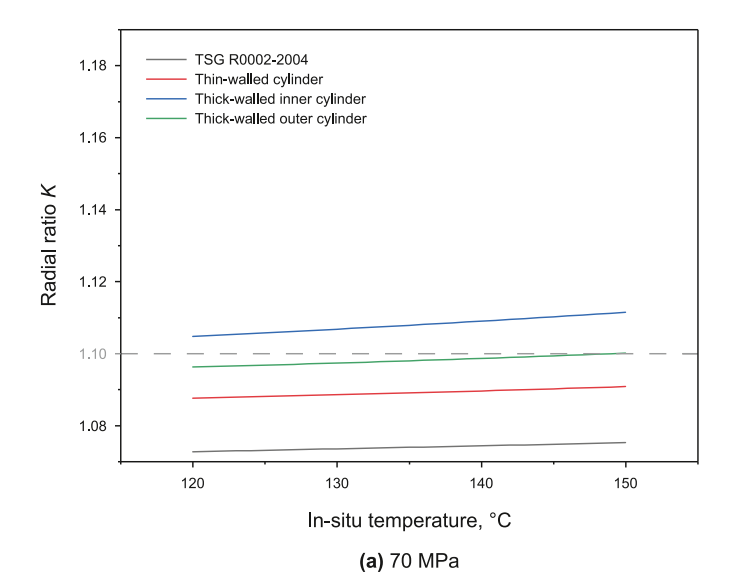
It is noteworthy that K exhibits greater sensitivity to in-situ pressure than to in-situ temperature, as shown in Fig. 3. When K is calculated at different pressure levels, the fluctuation range of *K* is small under temperature change. Therefore, designing the temperature-preserved core chamber based on in-situ pressure rather than in-situ temperature leads to more efficient space utilization. According to the Special Equipment Safety Design Code TSG R0002-2004, the effect of temperature is considered a strength reduction factor. The diameter ratio curve calculated based on this design principle was compared with the diameter ratio curve derived in this study, as shown in Fig. 4. It can be seen that, under the same safety factor, the diameter ratio K calculated by the design criteria derived using the Lame formula and thermal stress in this study are safer than the requirements of the design code, thus demonstrating the reasonableness and safety of this diameter ratio curve.

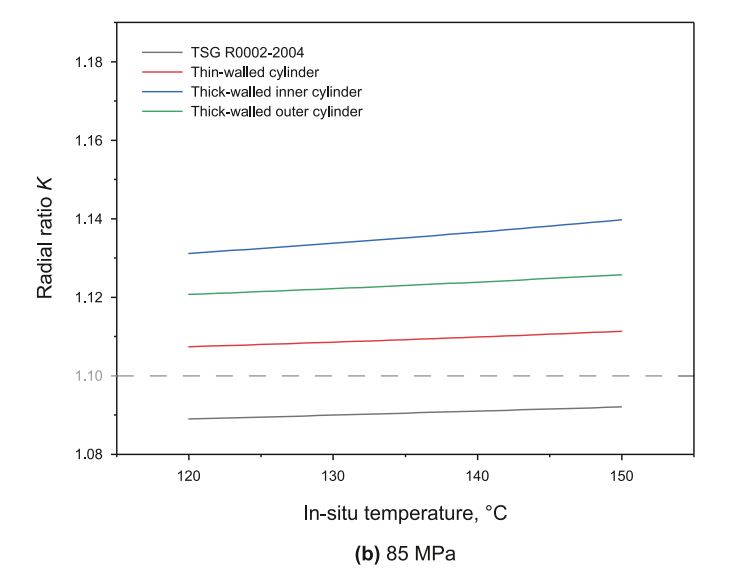
The comparison of *K*-value calculation results across the three design methods in this study reveals that for both 85 and 100 MPa pressures, the *K*-values for all cylinders exceed 1.1. Consequently, the inner and outer cylinders should be designed according to the thick-walled cylinder theory at these pressures. In contrast, at 70 MPa, the *K*-values for the outer cylinder are below 1.1, indicating that the thin-walled cylinder theory should be applied for its design at this pressure. However, for the inner cylinder at 70 MPa, the *K*-values calculated using the thin-walled theory remain below 1.1, while those calculated with the thick-walled cylinder theory exceed 1.1. Following a conservative design approach, it is recommended that the inner cylinder be designed using the thick-walled cylinder theory at 70 MPa. Fig. 5 summarizes the design method selection for inner and outer cylinders under varying temperature-pressure coupling conditions.

Based on the selected design method and considering the stability criterion, the design wall thickness of the inner and outer cylinder of the temperature-preserved core chamber under different temperature-pressure coupling conditions are calculated, as shown in Table 4.

4. Mechanical properties of the temperature-preserved core chamber

In the previous section, we presented the design and calculations for temperature-preserved core chambers and determined the wall thicknesses for chambers rated at 70, 85, and 100 MPa. This section focuses on simulating the static field of the temperature-preserved core chamber under different temperature-pressure coupling conditions. The mechanical properties are thoroughly analyzed to assess both the chamber body's structural integrity and the vacuum layer's sealing performance.





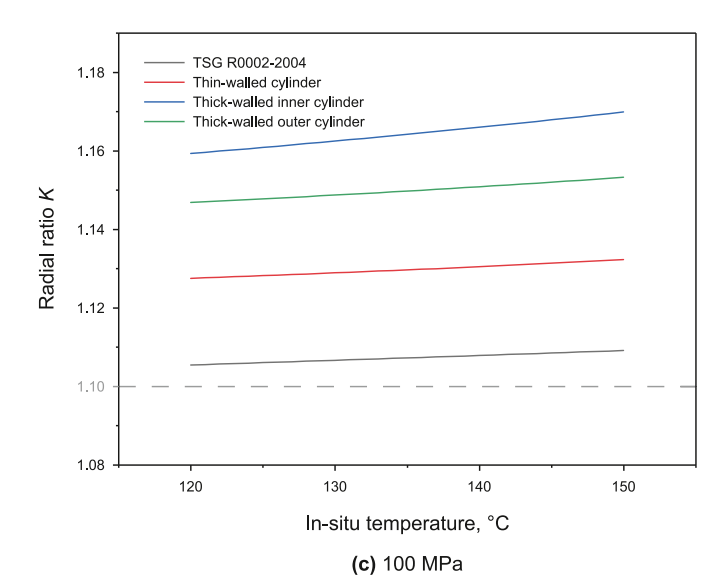


Fig. 4. Comparison of diameter ratio K calculation values using different design methods

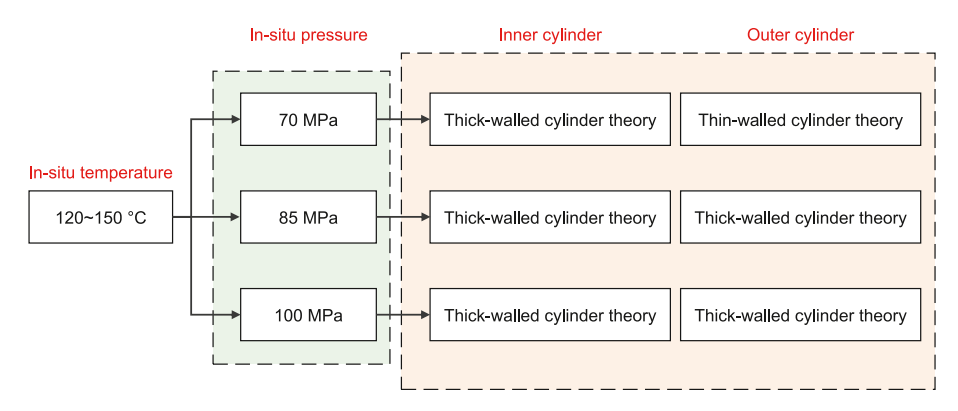


Fig. 5. Design methods selection for different temperature-pressure coupling environments.

Table 4Design value of the wall thickness for the temperature-preserved core chamber cylinders.

In-situ temperature, °C	In-situ pressure, MPa	Inner cylinder, mm	Outer cylinder, mm
120-150	70	3.49	4.58
120-150	85	4.37	6.15
120-150	100	5.31	7.31

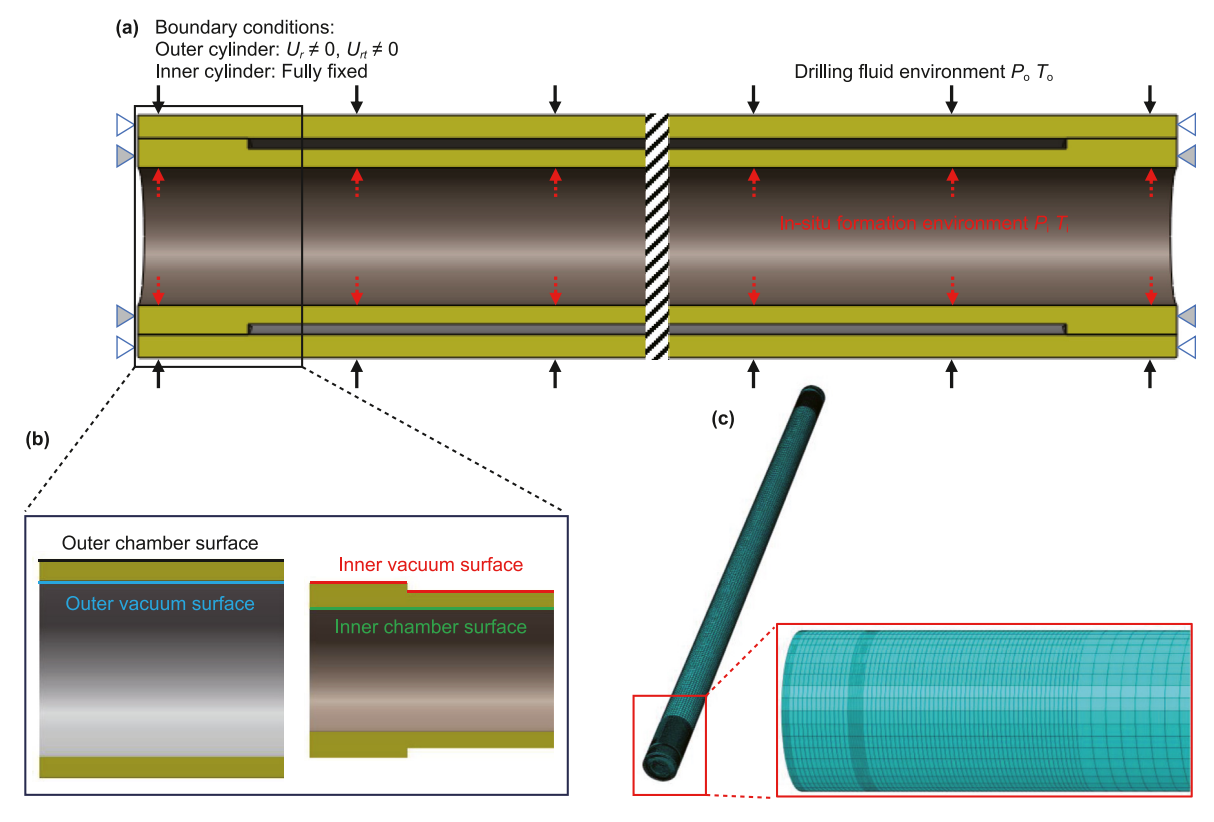


Fig. 6. Numerical model of the temperature-preserved core chamber: (a) boundary conditions; (b) measurement lines; (c) model meshing.

4.1. Numerical model construction

The two sealing regions each have a length of 50 mm. A damping coefficient 0.2 is applied in the tangential direction within these regions, while a "hard" contact condition is imposed in the normal direction. The vacuum section, located at the center of the core chamber, spans a length of 2500 mm. The diameter of the cylinder body is consistent with the specifications outlined in Section 3.3.

The boundary conditions are as follows:

(1) The ends of the inner cylinder are fully constrained, while the outer cylinder is connected to the inner cylinder through a fitting relationship, permitting radial displacement and circumferential rotation at the end face of the outer cylinder.

Table 5Key dimensions and parameters of the numerical model.

Parameter	Symbol	Value
Material density	ρ	7850 kg/m ³
Coefficient of heat conduction	λ	50 W/(m·K)
Specific heat	С	460 J/(kg·K)
Coefficient of thermal expansion	α	$1.2 \times 10^{-5} / K$
Elasticity modulus	Ε	210 GPa
Poisson ratio	μ	0.3
Yield strength	$R_{\rm e}$	830 MPa

- (2) Pressure: Surface pressures, denoted as p_0 and p_i , are applied to the outer surface of the outer cylinder and the inner surface of the inner cylinder, respectively.
- (3) Temperature field: An initial temperature T is applied to the temperature-preserved core chamber, while the external ambient temperature T_0 applied to the outer surface of the outer cylinder. Additionally, the in-situ ambient temperature T_1 applied to the inner surface of the inner cylinder.

To facilitate analysis, four measurement lines were established at key spatial positions within the temperature-preserved core chamber: the outer chamber surface, the outer vacuum surface, the inner vacuum surface, and the inner chamber surface. A schematic of the boundary conditions and the arrangement of the measurement lines is provided in Fig. 6. The material used in the model is 42CrMo alloy steel, and its key physical properties are listed in Table 5.

42CrMo steel is known for its outstanding strength and toughness. After heat treatment, it can achieve a hardness of up to 56 HRC (Jiang et al., 2014). Additionally, it demonstrates good wear resistance under high-temperature and high-pressure conditions (Zhang et al., 2021). The presence of chromium and manganese imparts a certain level of corrosion resistance, and using 42CrMo steel for tool manufacturing is cost-effective.

4.2. Stress characteristics of the temperature-preserved core chamber under different conditions

Irreversible plastic deformation and the resulting residual

stresses significantly impact the safety and longevity of the temperature-preserved core chamber. Consequently, analyzing the stress distribution within the chamber body is imperative. As shown in Fig. 7, the stress distribution exhibits significant variation at the chamber's ends, while it remains relatively stable in the central region. In particular, the stress in the 0–50 mm connection region at the ends of the chamber shows substantial fluctuations. Beyond the 50 mm mark, in the vacuum section, stress increases uniformly across all four surfaces, rapidly reaching a peak within a short distance before gradually decreasing. In contrast, stress remains stable in the middle of the chamber. This stress distribution pattern is similar to the results reported by Lotfi et al. (2023) in their study of stress distribution in cylindrical pressure vessels under mechanical and thermal loads. Since the stress remains stable in the middle section, the key stress variation and concentration occur at the ends of the chamber. Therefore, we focus our analysis on the region spanning 0-200 mm along the z-axis, delineated by the green shaded area in Fig. 7.

For this study, the stress caused by boundary effects should be ignored. Fig. 8 illustrates the stress distribution within the temperature-preserved core chambers. At an in-situ temperature of 120 °C, the maximum stresses of the 70, 85, and 100 MPa class temperature-preserved core chambers are 764.6, 758.3, and 758.7 MPa, respectively. As the in-situ temperature rises to 150 °C, the maximum stresses increase to 816.2, 806.6, and 806.0 MPa, respectively. Under all conditions designed and simulated in this study, the maximum stress of the temperature-preserved core chamber does not exceed the yield strength, meaning that the chamber remains in the elastic deformation phase during a single coring operation. This ensures that no plastic deformation occurs within the chamber, and no residual strain will develop after the coring is completed. Therefore, as designed in this study, the temperature-preserved core chamber can maintain its bearing performance and structural stability even under long-term cyclic temperature and pressure loads over multiple coring operations.

To analyze the impact of various temperature-pressure coupling conditions on the stress distribution characteristics of the temperature-preserved core chamber, we conducted a comparative assessment of the maximum von Mises stress on the four surfaces, as shown in Fig. 9. It can be seen that when the in-situ pressure is 70 MPa, the maximum stress surface of the chamber body is the

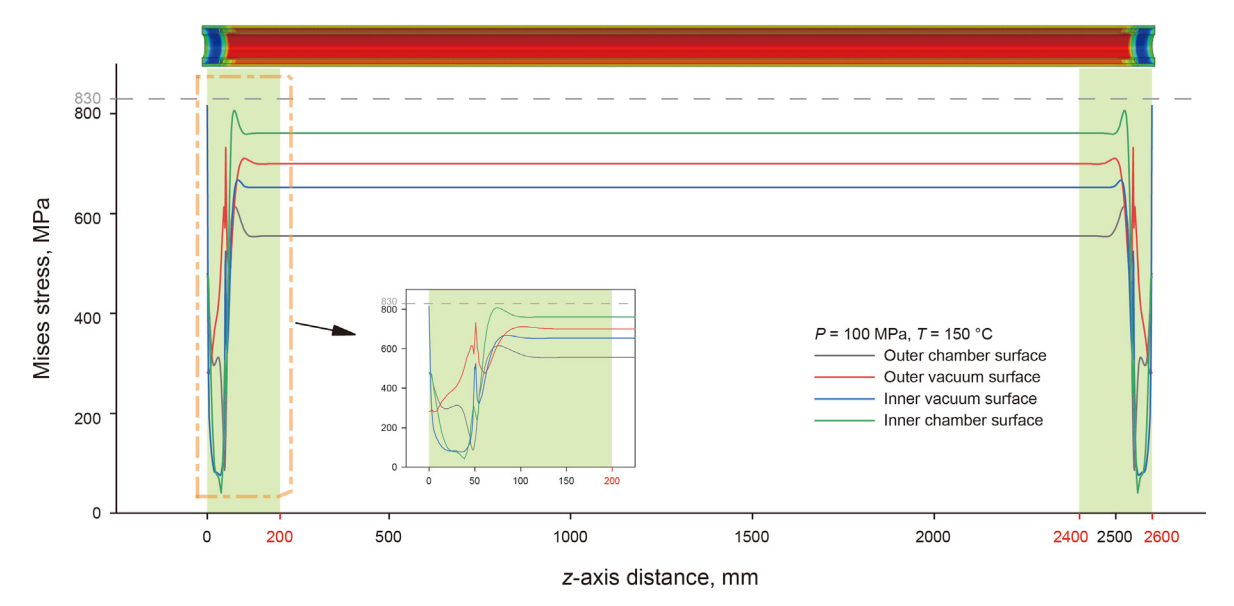


Fig. 7. Stress distribution curves and global stress cloud of the temperature-preserved core chamber at 150 °C and 100 MPa.

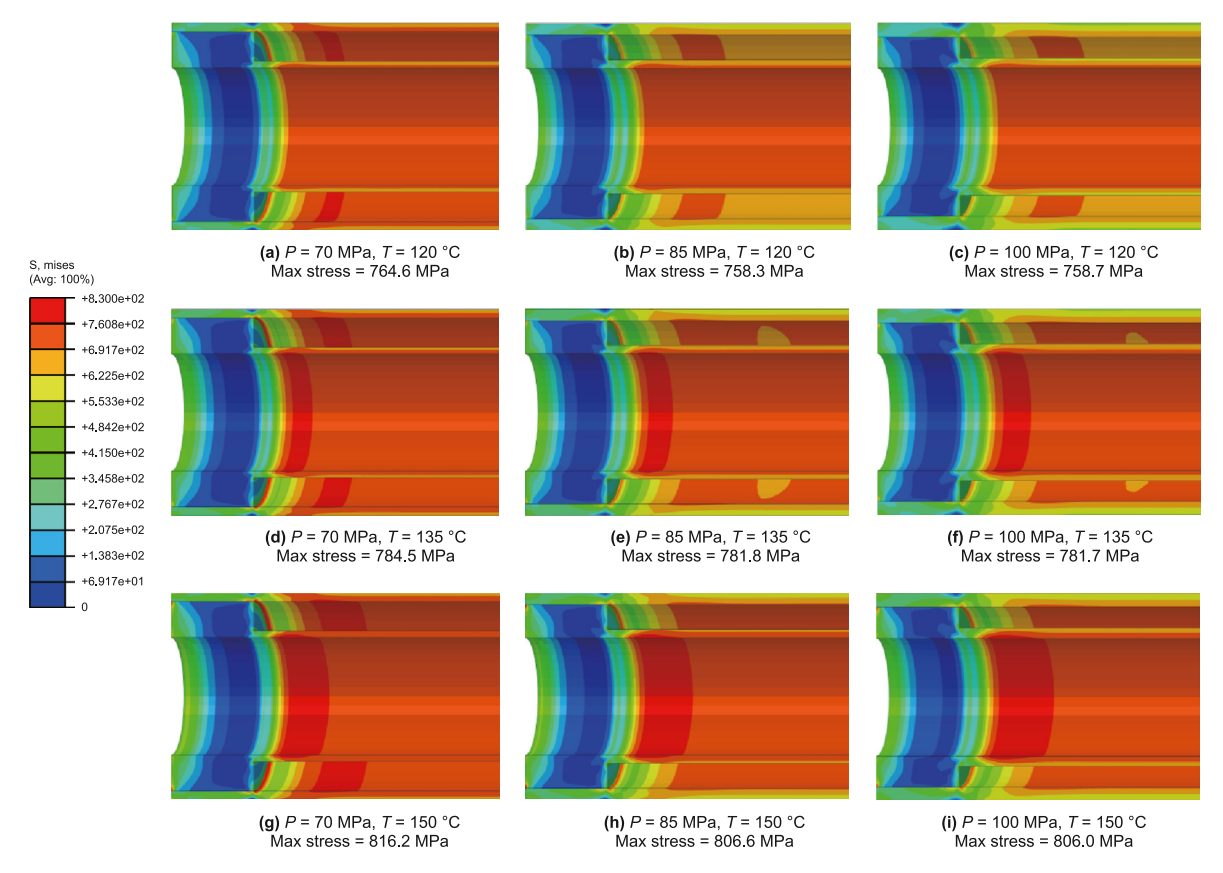


Fig. 8. Stress distribution cloud diagram in the 0–200 mm region along the z-axial of the temperature-preserved core chambers under different temperature-pressure coupling conditions.

outer vacuum surface. As the in-situ pressure increases, the stresses on the outer chamber surface, outer vacuum surface, and inner vacuum surface decrease. The inner chamber surface becomes the maximum stress surface of the chamber body. Notably, when the in-situ pressure increases from 70 to 100 MPa, the maximum stress on the outer chamber surface decreases significantly, with an average stress reduction of 15.5%. At this time, the stresses on the inner vacuum surface and the inner chamber surface are minimal, indicating that the inner cylinder has a higher mechanical capacity than the outer cylinder under these conditions. As the in-situ temperature increases, surface stresses also rise, although the difference in the increase is slight. Between 120 and 150 °C, the most significant increase in stress is observed on the inner vacuum surface, where it rises by 7.4%.

Fig. 10 shows the z-axis distance of the maximum stress point of each surface. The maximum stress points for the outer chamber surface, inner vacuum surface, and inner chamber surface are located within the 70-85 mm range, while the maximum stress point on the outer vacuum surface lies between 90 and 100 mm and 51 mm. When considered in conjunction with Fig. 8, it becomes apparent that stress concentrations occur on both the outer vacuum surface and the inner chamber surface. As a result, the mechanical capacity of the chamber has not been fully utilized. Specifically, high temperature induces axial expansion of the temperature-preserved core chamber for the inner chamber surface. Because the two ends of the temperature-preserved core chamber are limited by axial displacement, and the wall thickness of the fitting part is significantly higher than that of the vacuum part, severe extrusion occurs in the vacuum part near the fitting part, resulting in stress concentration. For the outer vacuum surface, increased temperature leads to radial expansion at the fitting part, which causes the inner cylinder to exert a jacking effect on the outer cylinder, further concentrating stress at the end of the fitting part. This stress concentration can be alleviated by chamfering the inner cylinder at the fitting part and adding a support ring at the maximum stress point, enhancing the mechanical capacity of the temperature-preserved core chamber.

4.3. Deformation characteristics of the temperature-preserved core chamber under different conditions

The sealing property of the vacuum layer is the decisive factor to ensure the temperature-preserved effect. Extreme temperaturepressure coupling conditions and intense mechanical vibrations from downhole drilling tools will lead to sealing gaps in the fitting part. The reduced distance between the inner and outer vacuum surfaces may cause them to come into contact, compromising the temperature-preserved function. Therefore, a detailed analysis of the displacement distribution within the temperature-preserved core chamber is essential. Compared to the stress distribution, the displacement distribution of the temperature-preserved core chamber is simpler. At the ends of the chamber, the displacement on all four surfaces increases with z-axis distance. However, in the vacuum section, the displacement values on the outer chamber surface and outer vacuum surface begin to decrease before rapidly reaching a peak across all four surfaces. In the central region of the chamber, displacement remains stable. This displacement distribution pattern is similar to the findings of Lotfi et al. (2023). Therefore, the region spanning 0-200 mm along the z-axis, delineated by the green shaded area in Fig. 11, is selected for this analysis.

Fig. 12 illustrates the radial displacement distribution cloud of the temperature-preserved core chambers. The maximum

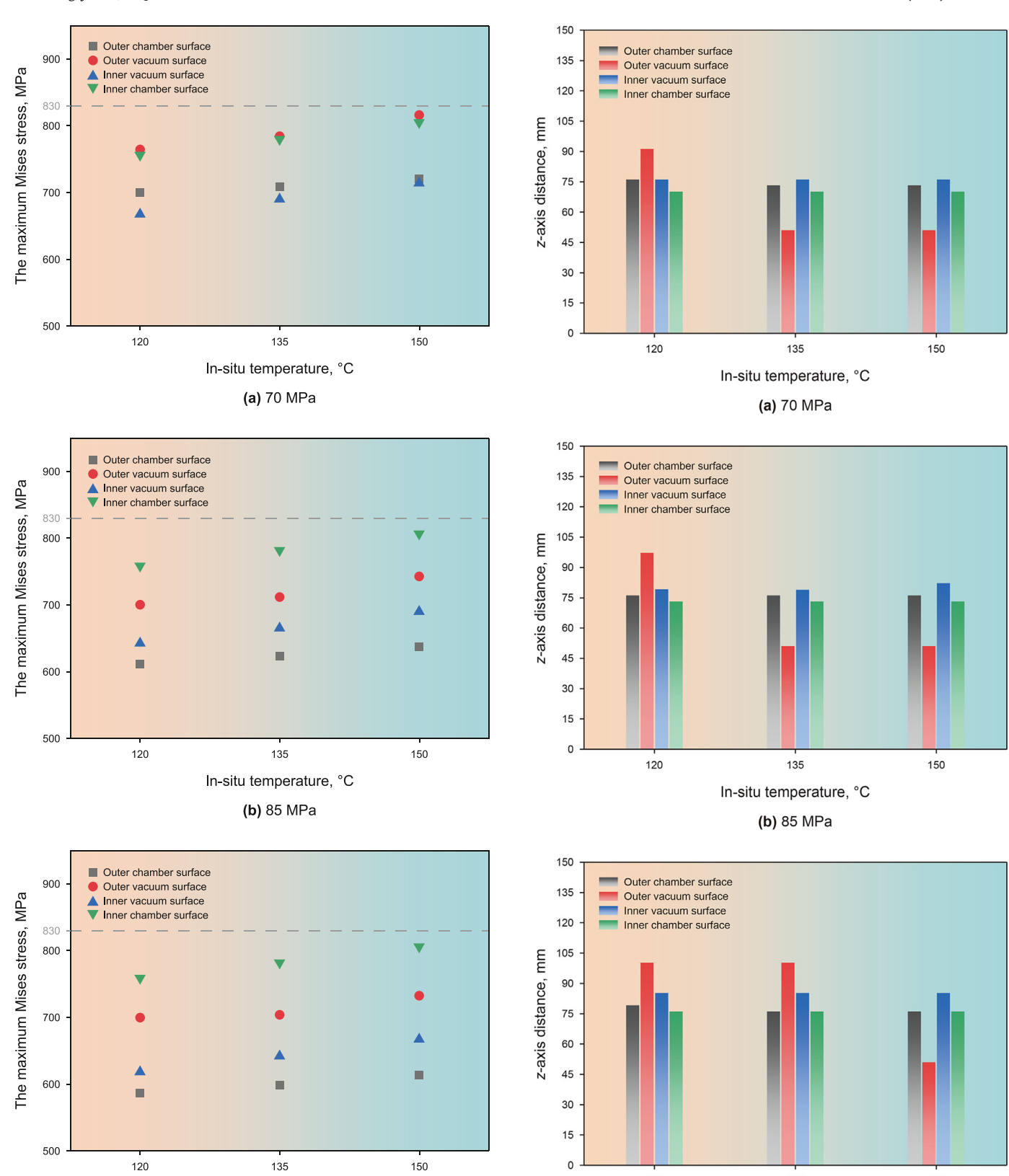


Fig. 9. Maximum stress on the four surfaces of the temperature-preserved core chambers under different temperature-pressure coupling conditions.

In-situ temperature, °C

(c) 100 MPa

Fig. 10. *z*-axis position of maximum stress points on the four surfaces of the temperature-preserved core chambers under different temperature-pressure coupling conditions.

In-situ temperature, °C

(c) 100 MPa

150

120

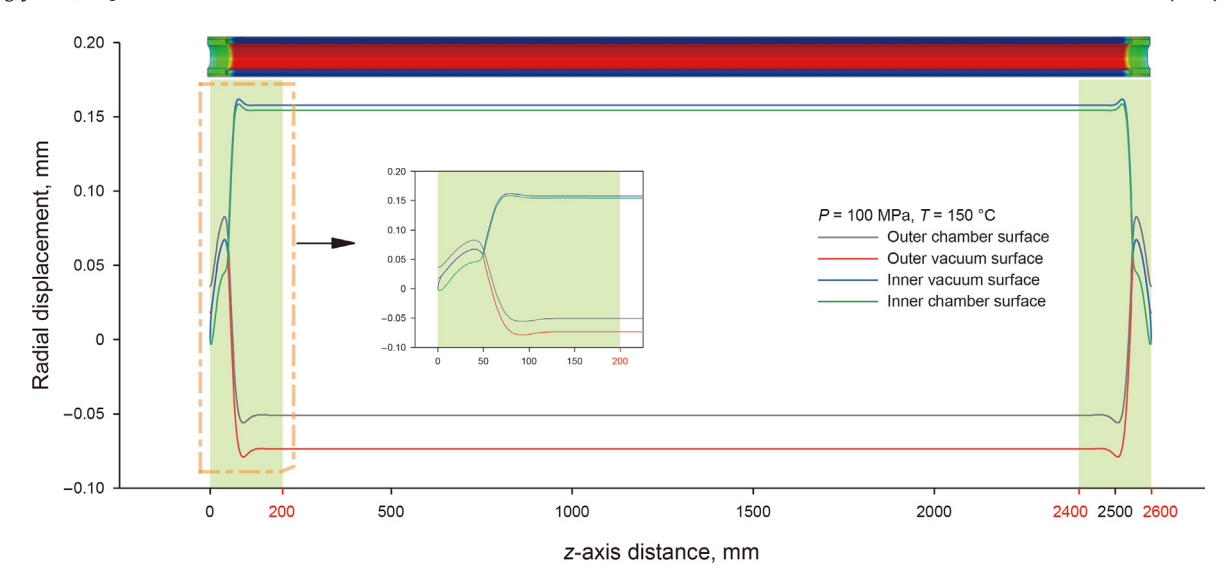


Fig. 11. Radial displacement distribution curves and global displacement cloud of the temperature-preserved core chamber at 150 °C and 100 MPa.

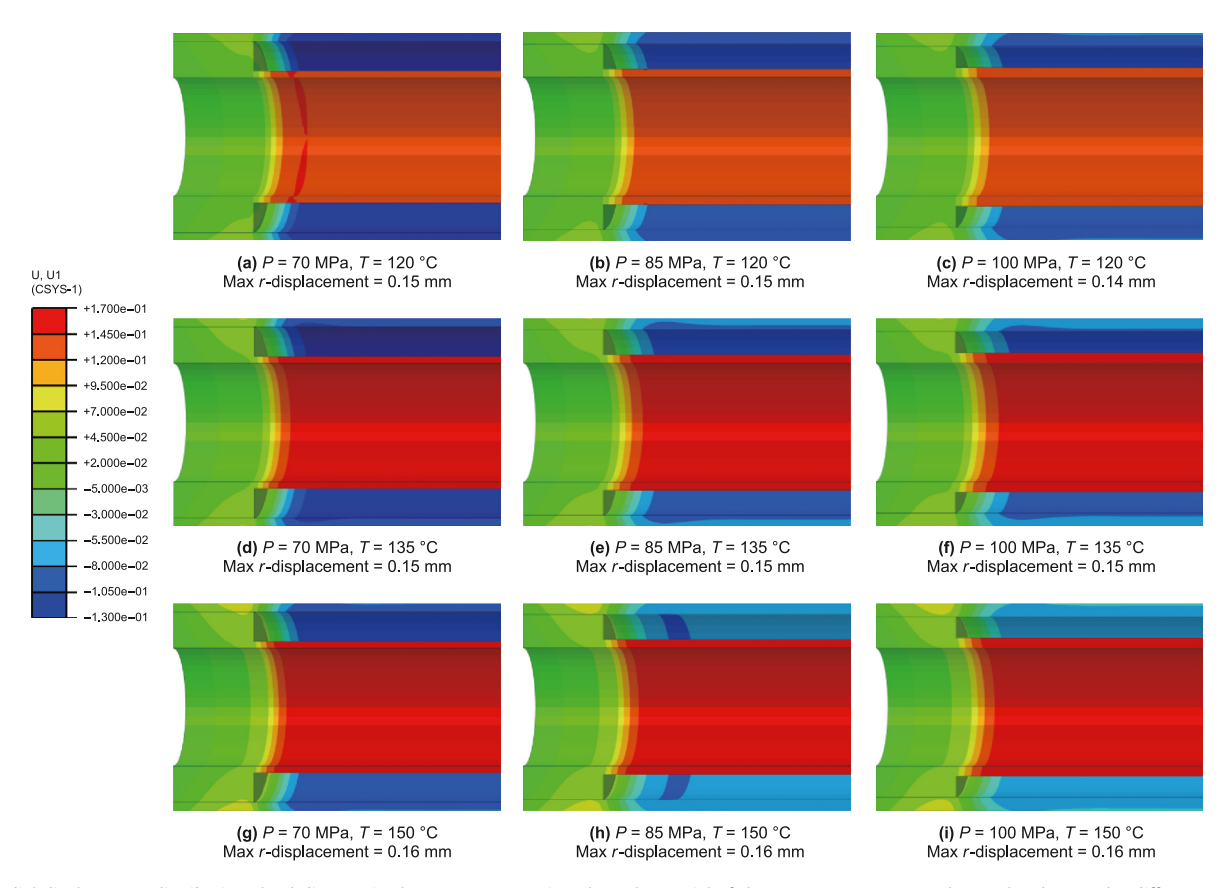


Fig. 12. Radial displacement distribution cloud diagram in the 0–200 mm region along the z-axial of the temperature-preserved core chambers under different temperature-pressure coupling conditions.

displacement occurs on the inner vacuum surface, ranging from 0.14 to 0.16 mm. As in-situ pressure increases, the wall thickness of the temperature-preserved core chamber increases, thereby reducing the displacement in the vacuum part of the outer cylinder. However, the displacement in the vacuum part of the inner cylinder shows minimal change. The increase in in-situ temperature will enhance the pushing force of the inner cylinder to the outer cylinder so that the displacement of the fitting part of the outer

cylinder increases and the displacement of the vacuum part of the outer cylinder decreases.

Fig. 13 shows the radial displacements of the outer and inner vacuum surfaces within the sealing part of the temperature-preserved core chamber under various temperature-pressure coupling conditions. The difference in displacement between the surfaces indicates the width of the sealing gap, while the length of this difference represents the sealing gap length. It can be seen that

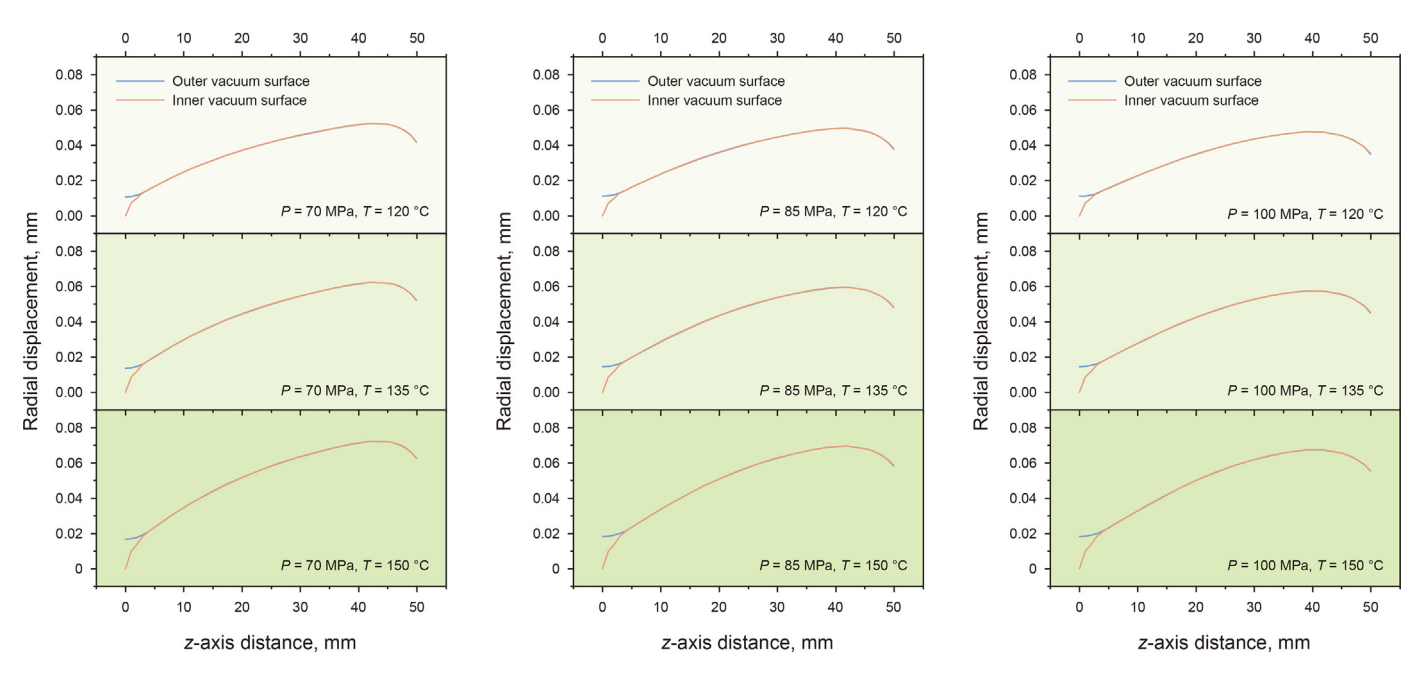


Fig. 13. Displacement of outer and inner vacuum surfaces in the sealing part of the temperature-preserved core chamber under different temperature-pressure coupling conditions.

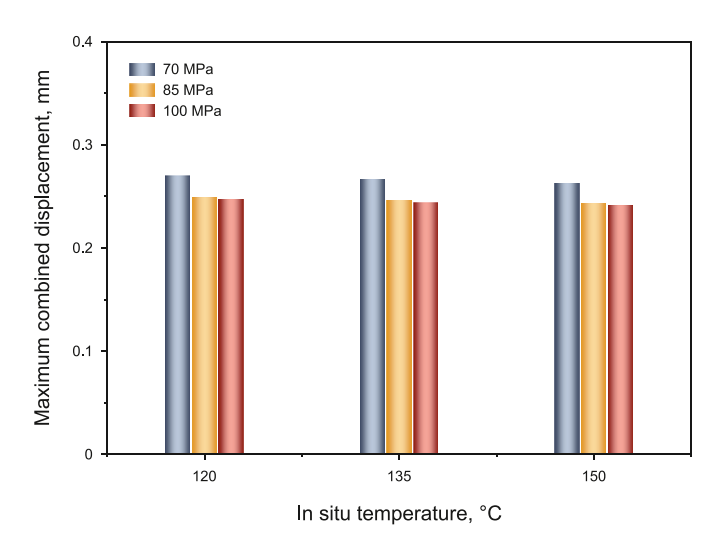


Fig. 14. Maximum combined displacement of vacuum layer surfaces under different temperature-pressure coupling conditions.

the sealing gap only appears on the outer side of the sealing part. As temperature increases, the radial displacement of the inner cylinder increases, leading to a wider sealing gap. The increase in pressure has little effect on the length and width of the sealing gap. Therefore, the sealing gap is mainly caused by thermal expansion. The maximum sealing gap does not exceed 5 mm in length and 0.02 mm in width. Consequently, the sealing ring should be positioned in the z-axis distance range of 5–50 mm, where no sealing gap occurs. As discussed in Section 4.2, the stress and strain of the temperature-preserved core chamber remain within the elastic range, ensuring no residual strain accumulates during multiple coring operations. Therefore, the sealing gap will not expand, and the vacuum seal will remain effective under long-term cyclic temperature and pressure loads. Fluor rubber is selected as the sealing material, given its resistance to temperature, oil, chemicals, and vacuum, as well as its excellent mechanical properties (Feng et al., 2023; Shi et al., 2024a; Sun et al., 2022; Wang et al., 2018).

Its tensile strength ranges from 10 to 20 MPa, elongation at break ranges from 150% to 350%, and tear strength ranges from 3 to 4 kN/m. Additionally, fluor rubber O-rings demonstrate excellent high-temperature sealing performance, maintaining a maximum leakage rate of 10^{-7} Pa · m³/s at 200 °C, with temperature resistance up to 204 °C (Liu et al., 2024; Wang et al., 2017). These properties make it ideal for long-term sealing in high-temperature and high-pressure environments.

To assess the potential risk of contact failure within the vacuum layer, we examine its deformation, represented by the maximum combined displacement of the vacuum layer surfaces, as shown in Fig. 14. The maximum combined displacement is between 0.24 and 0.27 mm. The increase in both in-situ temperature and in-situ pressure leads to a decrease in resultant displacement. Considering the thickness of the vacuum layer, this deformation is maximum, and there is no risk of contact between the vacuum layers.

As a result, the thickness of the vacuum layer can be reduced to allow for a larger core diameter. If the maximum surface displacement of the vacuum layer is denoted as u, the thickness of the anti-radiation material on the inner vacuum surface is h=1 mm, and the safety factor is 2, the required thickness of the vacuum layer can be derived:

$$H = 2(h+u) \tag{19}$$

The outer diameter of the inner cylinder can be expressed as:

$$r_0 = K_{\text{inner}}(D+C) \tag{20}$$

The relationship between the outer diameter of the outer cylinder and the maximum core diameter can be obtained:

$$R_{o} = K_{outer}[K_{inner}(D+C) + 2(h+u)]$$
(21)

$$D = \frac{R_0}{K_0 K_i} - \frac{2(h+u)}{K_i} - C \tag{22}$$

where r_0 is the outer diameter of the inner cylinder, K_{outer} is the outer cylinder diameter ratio, K_{inner} is the inner cylinder diameter

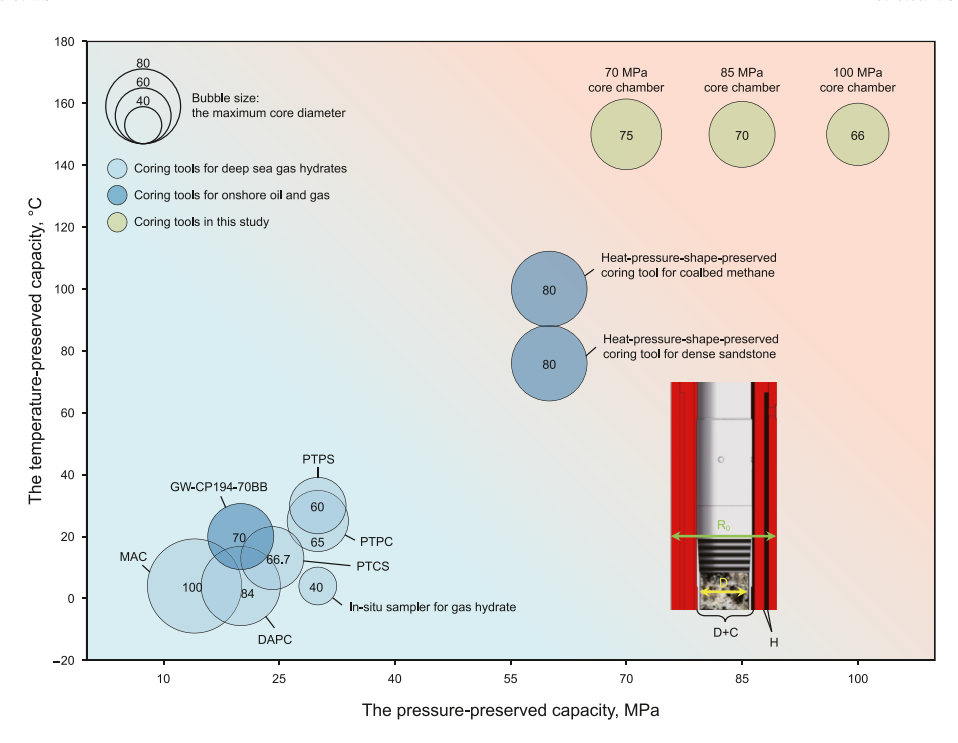


Fig. 15. Comparison of performance and core diameter across typical temperature-pressure preserved coring techniques.

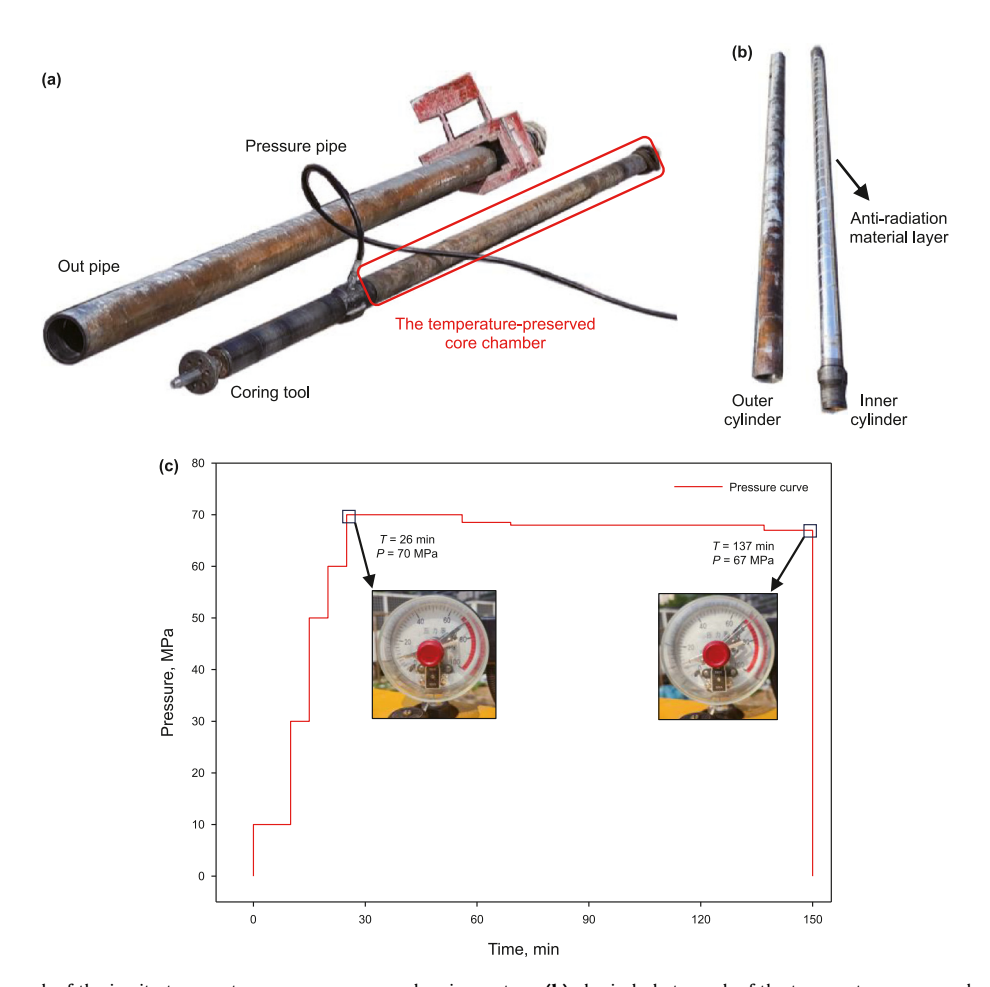


Fig. 16. (a) Physical photograph of the in-situ temperature-pressure preserved coring system; (b) physical photograph of the temperature-preserved core chamber; (c) pressure curve of the temperature-preserved core chamber.

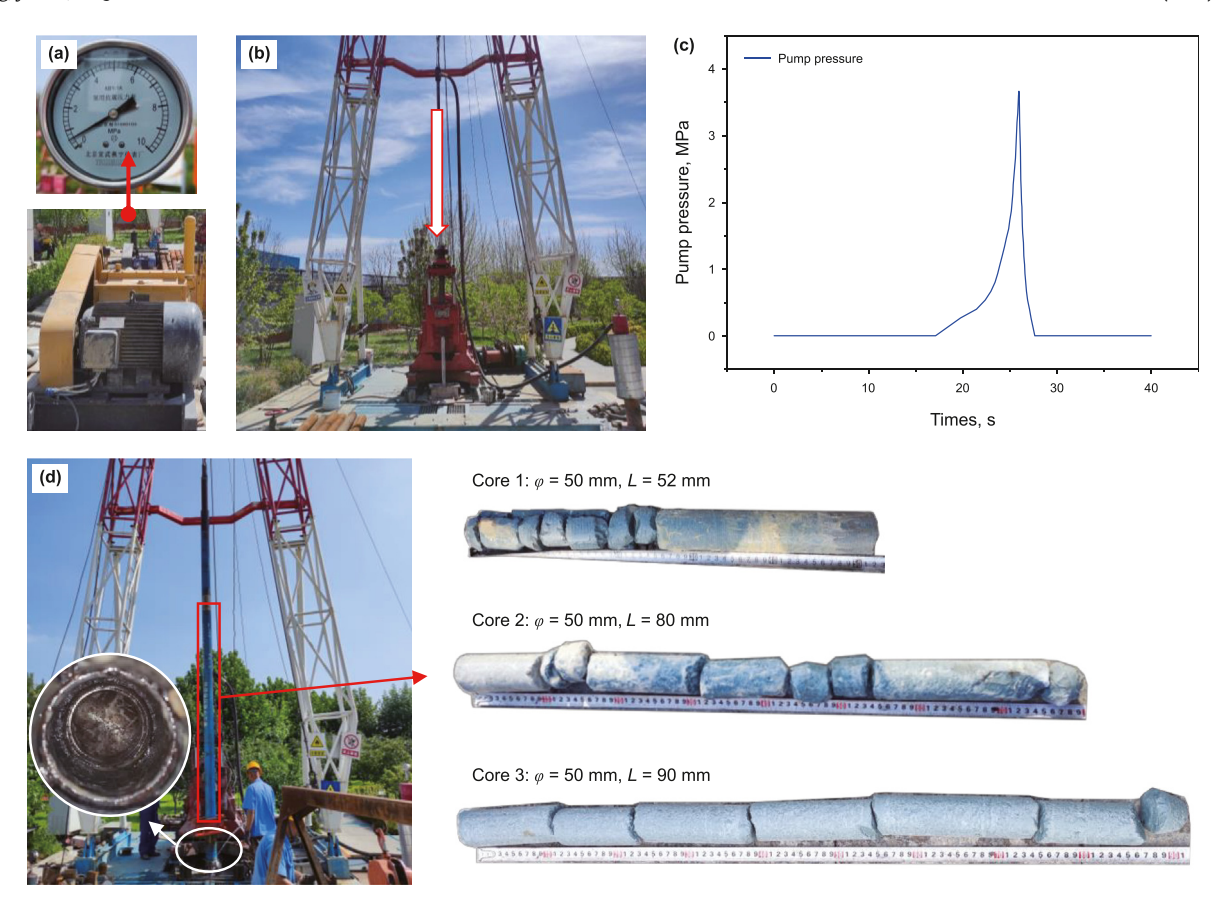


Fig. 17. (a) Loop test: circulation pump pressure stability at 0.4—0.6 MPa; (b) drilling and coring; (c) core temperature and pressure preservation: the pump indicator shows the core has entered the temperature-preserved core chamber; (d) lifting drill: the whole drill tool was raised to the wellhead, and the pressure controller was closed to show that the pressure had successfully preserved, the core lengths obtained in the three tests are 52, 80 and 90 mm respectively.

ratio, *D* is the maximum core diameter, and *C* is the constant.

Fig. 15 compares the temperature and pressure preservation performance and the maximum coring diameter of the temperature-preserved core chamber developed in this study with other typical coring tools. Among existing typical temperature-pressure preserved coring tools, the most advanced is the heat-pressure-shape-preserved coring tool for coalbed methane, with performance indicators of 76 °C and 60 MPa. However, the temperature-preserved core chamber developed in this study can withstand in-situ temperatures of up to 150 °C and pressures of up to 100 MPa, thus enabling coring operations under more extreme conditions than previous coring tools. Based on the derived maximum coring diameter formula, the temperature-preserved core chamber in this study allows for coring diameters of up to 75 mm for the 70 MPa class, 70 mm for the 85 MPa class, and 66 mm for the 100 MPa class.

In comparison with the maximum coring diameter of current typical coring tools, the temperature-preserved core chamber in this study significantly enhances temperature and pressure performance while still meeting the coring needs for large-diameter cores. Notably, compared to the PTPS and the heat-pressure-shape-preserved coring tool for dense sandstone, which uses composite insulation materials and active insulation devices, the temperature-preserved core chamber in this study relies solely on vacuum insulation, offering a simpler structure. After coring is completed, the temperature-preserved core chamber can be directly detached from the temperature-pressure preserved coring system for condition-preserved in-situ core cutting and testing operations. Therefore, the temperature-preserved core chamber

developed in this study offers superior temperature-preserved and pressure-preserved performance, excellent scalability for coring diameter design, and integrated condition-preserved core testing functionality.

5. Temperature-pressure preserved coring system integration tests

To address the critical challenges of preserving in-situ temperature and pressure during deep oil and gas coring, a design scheme for a temperature-preserved core chamber was developed to reliably procure in-situ cores. The design parameters of the temperature-preserved core chamber were determined through theoretical calculations. The static analysis of the temperature-preserved core chamber was conducted under different temperature-pressure coupling conditions using numerical simulation. Based on this, the 70 MPa class temperature-preserved core chamber prototype was produced and integrated into the in-situ temperature-pressure preserved coring system. This section describes the performance tests conducted following the system integration.

5.1. Pressure tolerance test

The image of the in-situ temperature-pressure preserved coring system prototype is displayed in Fig. 16(a). The temperature-preserved core chamber was integrated into the coring tool and connected to a pressure pump for pressurization. The disassembled temperature-preserved core chamber is displayed in Fig. 16(b). It

consists of an outer cylinder and an inner cylinder. In use, the antiradiation material is enwrapped around the inner cylinder. Subsequently, the inner cylinder is inserted into the outer cylinder to ensure a proper fit. Thereafter, the mating area is evacuated to create a vacuum insulation layer. A pressure tolerance test of 70 MPa was conducted to verify the pressure endurance capacity of the chamber. The pressure curve of the temperature-preserved core chamber is also shown in Fig. 16(c). The pressure was initially elevated to 10 MPa and maintained for an observational period of 10 min. Upon confirming the stability of the pressure without any fluctuations, a stepwise pressurization approach was implemented to increment the pressure to 70 MPa. Subsequently, the pressure was maintained at a constant level while its stability was continuously monitored. Eventually, once the pressure had remained stable for 120 min, the pressure was released. It should be noted that during the pressure-holding phase, the final pressure stabilized at 67 MPa, with pressure oscillations remaining within a 5% range. This minor deviation was attributed to the slight elastic deformation of the temperature-preserved core chamber.

5.2. Downhole coring test

The in-situ temperature-pressure preserved coring system was integrated and the coring function was tested on the self-developed in-situ coring test platform (Guo et al., 2024). In this test, the drilling fluid density was 1.2 g/cm³, and the viscosity was 57 s. The cement column was poured into the test well, and the test began after five days of cement curing. The test procedure, designed to simulate the real coring process, is outlined in the following steps and illustrated in Fig. 17. Firstly, a loop test was conducted. The temperature-pressure preserved coring system was lowered 20 m to the bottom of the well, and drilling fluid circulation was initiated. Circulation continued until the pump pressure stabilized between 0.4 and 0.6 MPa, as shown in Fig. 17(a). Next, drilling and coring operations were performed, as shown in Fig. 17(b). The drilling continued at the rated coring rate until the desired coring depth was achieved. Following this, core temperature and pressure preservation were implemented. The drill tool was lifted to extract the core, after which the hydrodynamic-driven differential motion assembly was triggered to lift the core tube into the temperaturepreserved core chamber. The pressure controller was then activated to seal the core chamber. The change in pump pressure, as shown in Fig. 17(c), confirms that the core tube successfully entered the temperature-preserved core chamber. Finally, the drill was lifted, completing the coring operation. The samples obtained from three coring function tests are shown in Fig. 17(d). The results of the coring function test verify that the core can be smoothly transferred into the temperature-preserved core chamber, and the integration of the temperature-pressure preserved coring system is feasible and effective.

6. Conclusions

To address the challenge of preserving in-situ temperature in high temperature-pressure environments, a novel temperature-preserved core chamber has been designed, capable of integration into an in-situ temperature-pressure preserved coring system. Numerical simulations and system integration tests were conducted to validate the design. The main conclusions are as follows:

(1) The composition and working principle of the new integrated temperature-pressure preserved coring system were analyzed. The temperature-preserved core chamber is connected to the hydrodynamic-driven differential motion assembly at its upper end and the pressure controller at its

lower end, allowing the core tube to pass through the chamber. The core chamber is insulated by a vacuum layer, formed by concentric cylinders, with the fitting parts sealed by the sealing ring. Upon lifting the core into the temperature-preserved core chamber, the system effectively minimizes circumferential heat loss.

- (2) The design principles for the temperature-preserved core chamber were established. Based on the Lamé equation and distortion energy theory, the diameter ratio *K* of the temperature-preserved chamber is determined by the insitu pressure level, optimizing space utilization. The inner and outer cylinders of the 70 MPa chamber are designed using thick-walled cylinder theory and thin-walled cylinder theory, respectively, while the 85 and 100 MPa chambers are designed entirely using thick-walled cylinder theory.
- (3) The mechanical properties of the temperature-preserved core chamber were analyzed based on numerical simulations. The results show that the maximum stresses for the 70, 85, and 100 MPa class chambers are 816.2, 806.6, and 806.0 MPa, respectively, with no plastic deformation occurring. Stress concentrations on the inner chamber surface and outer vacuum surface can be mitigated by chamfering the ends of the fitting part and incorporating support rings at the maximum stress points. These modifications enhance the mechanical strength of the temperature-preserved core chamber. The sealing gap appears only on the external sealing part with the maximum sealing gap not exceeding 5 mm in length and 0.02 mm in width. The maximum combined displacement is between 0.24 and 0.27 mm, indicating no risk of contact between the vacuum layers. The maximum core diameter for the three class temperaturepreserved core chambers is 73, 69, and 65 mm, which significantly improves temperature-pressure preserved performance while meeting the needs of large-diameter cores.
- (4) A prototype of the 70 MPa class temperature-preserved core chamber was produced, and the integrated temperaturepressure preserved coring system underwent pressure tolerance and coring function tests on the self-developed insitu coring test platform. The test results demonstrated that the system operates reliably at 70 MPa for 120 min, with pressure fluctuations maintained within an acceptable range of 5%. The temperature-preserved core chamber was found to integrate well with the original mechanical structure, allowing for the successful extraction of 50 mm diameter cores.

CRediT authorship contribution statement

Yi-Wei Zhang: Writing — original draft, Visualization, Validation, Software, Methodology, Investigation, Formal analysis, Data curation, Conceptualization. Jia-Nan Li: Writing — review & editing, Resources, Project administration, Conceptualization. Zhi-Qiang He: Supervision, Software. Ling Chen: Project administration, Methodology, Funding acquisition. Cong Li: Software, Conceptualization. Da Guo: Methodology, Conceptualization. Ding-Ming Wang: Investigation. Xin Fang: Software. He-Ping Xie: Resources, Project administration, Methodology, Funding acquisition, Conceptualization.

Conflict of interest

The authors declare that they have no known competing financial interests or personal relationships that could have appeared to influence the work reported in this paper.

Acknowledgments

The authors are grateful for the financial support from the National Key R&D Program of China (No. 2022YFB3706604), the National Natural Science Foundation of China (52304033), Sichuan Science and Technology Program (2023NSFSC0790), China Postdoctoral Science Foundation (No.2023M742446) and the National Natural Science Foundation of China (No. 51827901).

References

- Abegg, F., Hohnberg, H.J., Pape, T., et al., 2008. Development and application of pressure-core-sampling systems for the investigation of gas- and gas-hydrate-bearing sediments. Deep Sea Res. Oceanogr. Res. Pap. 55 (11), 1590–1599. https://doi.org/10.1016/j.dsr.2008.06.006.
- Dickens, Gerald, R., Paull, et al., 1997. Direct measurement of in situ methane quantities in a large gas-hydrate reservoir. Nature 385 (6615), 426–428. https://doi.org/10.1038/385426a0.
- Feng, H.F., Su, Y.X., Sun, C.C., et al., 2023. Progress and prospect of high temperature resistant perfluoroether rubber composites. Polym. Mater. Sci. Eng. 39 (7), 185–190. https://doi.org/10.16865/j.cnki.1000-7555.2023.0150 (in Chinese).
- Gao, M.Z., Wang, X., Zhang, G.Q., et al., 2022. The novel idea and technical progress of lunar in-situ condition preserved coring. Geomech. Geophys. Geo Energ. Geo Resour. 8 (2), 1–20. https://doi.org/10.1007/s40948-022-00350-0.
- Guo, D., Chen, L., Zhou, Z.Y., et al., 2023a. Development of a pressure coring system for the investigation of deep underground exploration. Int. J. Min. Sci. Technol. 33 (11), 1351–1364. https://doi.org/10.1016/j.ijmst.2023.10.001.
- Guo, D., Xie, H.P., Chen, L., et al., 2023b. In-situ pressure-preserved coring for deep exploration: insight into the rotation behavior of the valve cover of a pressure controller. Pet. Sci. 20 (4), 2386–2398. https://doi.org/10.1016/ j.petsci.2023.02.020.
- Guo, D., Xie, H.P., Gao, M.Z., et al., 2024. In-situ pressure-preserved coring for deep oil and gas exploration: design scheme for a coring tool and research on the insitu pressure-preserving mechanism. Energy 286, 129519. https://doi.org/ 10.1016/j.energy.2023.129519.
- Guo, X.S., Hu, D.F., Li, Y.P., et al., 2019. Theoretical progress and key technologies of onshore ultra-deep oil/gas exploration. Engineering 5 (3), 458–470. https:// doi.org/10.1016/j.eng.2019.01.012.
- He, Z.Q., Xie, H.P., Chen, L., et al., 2024. Research on thermal insulation materials properties under HTHP conditions for deep oil and gas reservoir rock ITP-Coring, Pet. Sci. 21 (4), 2625–2637. https://doi.org/10.1016/j.petsci.2024.03.005.
- He, Z.Q., Yang, Y., Yu, B., et al., 2022. Research on properties of hollow glass microspheres/epoxy resin composites applied in deep rock in-situ temperaturepreserved coring. Pet. Sci. 19 (2), 720–730. https://doi.org/10.1016/ i.petsci.2021.10.028.
- Hu, W., Xu, T., Yang, Y., et al., 2023. Fluid phases and behaviors in ultra-deep oil and gas reservoirs, Tarim Basin. Oil Gas Geol. 44 (4), 1044–1053. https://doi.org/10.11743/ogg20230419 (in Chinese).
- Jiang, B., Zhou, L., Wen, X., et al., 2014. Heat treatment properties of 42CrMo steel for bearing ring of varisized shield tunneling machine. Acta Metall Sin Engl Lett. 27 (3), 383–388. https://doi.org/10.1007/s40195-014-0062-2.
- Júnior, M.T., Zilio, G., Mortean, M.V.V., et al., 2023. Experimental and numerical analysis of transient thermal stresses on thick-walled cylinder. Int. J. Pres. Ves. Pip. 202, 104884. https://doi.org/10.1016/j.ijpvp.2023.104884.
- Kawasaki, M., Umezu, S., Yasuda, M., 2006. Pressure temperature core sampler (PTCS). J. Jpn. Assoc. Pet. Technol. 71 (1), 139–147. https://doi.org/10.3720/iant.71139
- Kvenvolden, K.A., Barnard, L.A., Cameron, D.H., 1983. Pressure core barrel: application to the study of gas hydrates, deep sea drilling project site 533, Leg 76. Initial. Reports DSDP. 76, 367–375. https://doi.org/10.2973/dsdp.proc.76.107.1983.
- Liu, Z.X., Zou, W., Wang, C., et al., 2024. Development and application of a new type of open hole packer for ultra-high-temperature and high-pressure wells. Construction Machinery and Equipment 55 (4), 23–29. https://doi.org/10.3969/ i.issn.1000-1212.2024.04.006 (in Chinese).
- Lotfi, M., Loghman, A., Arefi, M., 2023. Thermo-elastic analysis of functionally graded porous thick-walled cylindrical pressure vessels with variable thickness subjected to mechanical and thermal loading by higher-order shear deformation theory. Int. J. Pres. Ves. Pip. 205, 105012. https://doi.org/10.1016/j.ijpvp.2023.105012.
- Ma, Y.S., Cai, X.Y., Li, H.L., et al., 2023. New insights into the formation mechanism of deep-ultra-deep carbonate reservoirs and the direction of oil and gas exploration in extra-deep strata. Earth Sci. Front. 30 (6), 1–12. https://doi.org/10.13745/j.esf.sf.2023.2.35 (in Chinese).
- Milkov, A.V., Dickens, G.R., Claypool, G.E., et al., 2004. Co-existence of gas hydrate, free gas, and brine within the regional gas hydrate stability zone at Hydrate Ridge (Oregon margin): evidence from prolonged degassing of a pressurized core. Earth Planet Sci. Lett. 222 (3–4), 829–843. https://doi.org/10.1016/i.epsl.2004.03.028.
- Qin, H.W., Gu, L.Y., Li, S.L., et al., 2005. Pressure tight piston corer-a new approach on gas hydrate investigation. China Ocean Eng. 19 (1), 121–128. https://doi.org/

10.3321/j.issn:0890-5487.2005.01.011.

- Schultheiss, P., Holland, M., Humphrey, G., 2009. Wireline coring and analysis under pressure: recent use and future developments of the HYACINTH system. Sci. Drill. 7, 44–50. https://doi.org/10.5194/sd-7-44-2009.
- Şeker, B.Ş., Gökçe, M., Toklu, K., 2022. Investigation of the effect of silica fume and synthetic foam additive on cell structure in ultra-low density foam concrete. Case Stud. Constr. Mater. 16, e01062. https://doi.org/10.1016/ j.cscm.2022.e01062.
- Shi, X.J., Xie, H.P., Li, C., et al., 2024a. Performance of a deep in situ pressure-preserving coring controller in a high-temperature and ultrahigh-pressure test system. J. Rock Mech. Geotech. Eng. 17 (2), 877–896. https://doi.org/10.1016/i.jrmge.2024.01.012.
- Shi, X.J., Xie, H.P., Li, C., et al., 2024b. Influence of the mechanical properties of materials on the ultimate pressure-bearing capability of a pressure-preserving controller. Pet. Sci. 21 (5), 3558–3574. https://doi.org/10.1016/ i.petsci.2024.04.003.
- Sun, Y.T., Lu, D.S., Liu, L., et al., 2022. Research progress in applications of fluororubber nanocomposites. China Plast. 36 (12), 167–174. https://doi.org/10.19491/ i.issn.1001-9278.2022.12.022 (in Chinese).
- Wang, C.S., Ming, C.Z., Zhang, H., et al., 2024. Analysis of secondary makeup characteristics of drill collar joint and prediction of downhole equivalent impact torque of Well SDTK1. Petrol. Explor. Dev. 51 (3), 697–705. https://doi.org/10.11698/PED.20240057 (in Chinese).
- Wang, D.W., Tang, S.Y., Zhang, D.Z., et al., 2017. Experimental investigations on high temperature performance of fluorine rubber ring of explosion vessel (1). Pressure Vessel Technology 34 (8), 7–11+56. https://doi.org/10.3969/j.issn. 1001-4837.2017.08.002 (in Chinese).
- Wang, H.G., Huang, H.C., Bi, W.X., et al., 2022a. Deep and ultra-deep oil and gas well drilling technologies: Progress and prospect. Nat. Gas. Ind. B 9 (2), 141–157. https://doi.org/10.1016/J.NGIB.2021.08.019.
- Wang, J.C., Deng, X.F., Zeng, D.Z., et al., 2018. Corrosion mechanism of terafluoroethylene-propylene rubber O-ring in simulated wellbore condition. Chem. Eng. Oil Gas 47 (4), 77–82. https://doi.org/10.1016/j.corsci.2016.02.028 (in Chinese).
- Wang, X.G., Zou, D.Y., Yang, L.W., et al., 2022b. Optimization and application in unconventional oil and gas development of heat-pressure-shape-preserved coring tool. China Petrol. Mach. 50 (2), 109–114. https://doi.org/10.16082/j.cnki.issn.1001-4578.2022.02.016 (in Chinese).
- Wang, X.G., Zou, D.Y., Yang, L.W., et al., 2021. Development and field application of a coalbed methane coring tool with pressure maintenance, thermal insulation, and shape preservation capabilities. Petrol. Drill. Tech. 49 (3), 94–99. https:// doi.org/10.11911/syztjs.2021061 (in Chinese).
- Xie, H.P., Cui, P.F., Shang, D.L., et al., 2023a. Research advances on the in-situ pressure-preserved coring and gas parameter determination for deep coal seams. Coal Geol. Explor. 51 (8), 1–12. https://doi.org/10.12363/issn.1001-1986.23.02.0075 (in Chinese).
- Xie, H.P., Gao, M.Z., Zhang, R., et al., 2020. Study on concept and progress of in situ fidelity coring of deep rocks. Chin. J. Rock Mech. Eng. 39 (5), 865–876. https://doi.org/10.13722/j.cnki.jrme.2020.0138 (in Chinese).
- Xie, H.P., Gao, M.Z., Zhang, R., et al., 2018. Study on the mechanical properties and mechanical response of coal mining at 1000 m or deeper. Rock Mech. Rock Eng. 52 (5), 1475–1490. https://doi.org/10.1007/s00603-018-1509-y.
- Xie, H.P., Hu, Y.Q., Gao, M.Z., et al., 2023b. Research progress and application of deep in-situ condition preserved coring and testing. Int. J. Min. Sci. Technol. 33 (11), 1319–1337. https://doi.org/10.1016/j.ijmst.2023.06.007.
- Xie, H.P., Konietzky, H., Zhou, H.W., 2019. Special issue "deep mining." Rock Mech. Rock Eng. 52 (5), 1415–1416. https://doi.org/10.1007/s00603-019-01805-9.
- Xie, H.P., Liu, T., Gao, M.Z., et al., 2021. Research on in-situ condition preserved coring and testing systems. Pet. Sci. 18 (6), 1840–1859. https://doi.org/10.1016/ i.petsci.2021.11.003.
- Xue, S.N., He, Z.Q., Li, C., et al., 2023. Physical and mechanical properties of thermal insulation materials for in-situ temperature-preserved coring of deep rocks. Coal Geol. Explor. 51 (8), 30–38. https://doi.org/10.12363/issn.1001-1986.22.12.0938 (in Chinese).
- Yang, J.P., Chen, L., Gu, X.B., et al., 2022. Hollow glass microspheres/silicone rubber composite materials toward materials for high performance deep in-situ temperature-preserved coring. Pet. Sci. 19 (1), 309—320. https://doi.org/10.1016/ j.petsci.2021.11.012.
- Yang, L.W., Su, Y., Luo, J., et al., 2020. Development and application of GW-CP194-80A pressure-maintaining coring tool. Nat. Gas. Ind. 40 (4), 91–96. https://doi.org/10.3787/j.issn.1000-0976.2020.04.011 (in Chinese).
- Yang, L.W., Sun, W.T., Luo, J., et al., 2014. Study and application of GWY194-70BB heat and pressure preservation coring tool. Oil Drill. amp; Product. Technol. 36 (5), 58–61. https://doi.org/10.13639/j.odpt.2014.05.014 (in Chinese).
- Zhang, H.D., Yan, X.G., Chen, Z., et al., 2021. Effects of thermo-mechanical treatment on hardness, wear resistance, impact toughness and microstructure of 42CrMo steel. Hot Working Technology 50 (22), 125–127+131. https://doi.org/10.14158/j.cnki.1001-3814.20211195 (in Chinese).
- Zhang, H.J., Liu, C.L., Wang, X.Z., et al., 2007a. Application of submerged pressure maintaining sealed coring techniques to Well Xushen-12. Oil Drilling & Production Technology 29 (4), 110–111+114. https://doi.org/10.3969/j.issn.1000-7393.2007.04.033 (in Chinese).
- Zhang, Y.Q., Sun, J.H., Zhao, H.T., et al., 2007b. Test research on in-situ sampler for gas hydrate. Drill. Eng. 34 (9), 62–65. https://doi.org/10.3969/j.issn.1672-7428.2007.09.017 (in Chinese).

- Zhang, Z.Y., Zhu, G.Y., Zhang, Y.J., et al., 2018. The origin and accumulation of multiphase reservoirs in the east Tabei uplift, Tarim Basin, China. Mar. Petrol. Geol. 98, 533–553. https://doi.org/10.1016/j.marpetgeo.2018.08.036.
- Zhao, Y., Liu, H.L., Cai, J.P., et al., 2023. Development and application of TKP194-80 sealed pressure-holding coring tool. Drill. Eng. 50 (4), 77–83. https://doi.org/10.12143/j.ztgc.2023.04.011 (in Chinese).

 Zhu, G.Y., Zhang, Y., Zhou, X.X., et al., 2019. TSR, deep oil cracking and exploration potential in the Hetianhe gas field, Tarim Basin, China. Fuel 236, 1078–1092.
- https://doi.org/10.1016/j.fuel.2018.08.119.
- Zhu, H.Y., Liu, Q.Y., Deng, J.G., et al., 2011. Pressure and temperature preservation techniques for gas-hydrate-bearing sediments sampling. Energy 36 (7), 4542-4551. https://doi.org/10.1016/j.energy.2011.03.053.
- Zhu, X.H., Li, K., Li, W.Z., et al., 2024. Drill string mechanical behaviors of large-size borehole in the upper section of a 10000 m deep well. Nat. Gas. Ind. 44 (1), 49–57. https://doi.org/10.3787/j.issn.1000-0976.2024.01.005 (in Chinese).